MODELING OF ELECTROMAGNETIC STIRRING OF LIQUID METALS

A PROJECT REPORT

Submitted in partial fulfillment of the
Requirement for the award of the
Degree of

BACHELOR OF TECHNOLOGY
In
MECHANICAL ENGINEERING

By

YASH GANATRA
10BME 1043

Under the Guidance of

Dr. JayasankarVariyar

Dr. Pramod Kumar

SCHOOL OF MECHANICAL AND BUILDING SCIENCES
VIT University, CHENNAI
(Tamil Nadu) 600127
(MAY 2014)

VIT UNIVERSITY
(Estd. u/s 3 of UGC Act 1956)
www.vit.ac.in
Vellore ▪ Chennai
CHENNAI CAMPUS
Vandalur - Kelambakkam Road, Chennai - 600127

SCHOOL OF MECHANICAL AND BUILDING SCIENCES

CERTIFICATE

This is to certify that the project work titled "**MODELING OF ELECTROMAGNETIC STIRRING OF LIQUID METALS**" that is being submitted by ***"YASH GANATRA"*****(10BME 1043)** is in partial fulfillment of the requirement for the award of **Bachelor of Technology in Mechanical Engineering**, is a record of bonafide work done under my guidance. The contents of this project work, in full or in parts, have neither been taken from any other source nor have been submitted to any other Institute or University for award of any degree or diploma and the same is certified.

Thesis submission date: 14 MAY, 2014

Guide **Program Chair**

Internal Examiner **External Examiner**

To my Parents, without whose sacrifices and love,
I would not be here

ACKNOWLEDGEMENTS

It would be impossible and naïve of me to express my gratitude to all those who have supported me throughout my academic career. Nevertheless, I would like to show my appreciation by writing a few words.

No gratitude is enough to thank my parents for their unwavering support and love throughout. They have stood beside me whenever I was low on confidence and always let me choose my own path. Many a times, I have chosen the wrong one but their faith in me makes me believe that I can choose the right path.

I hope that my future studies will be blessed by teachers as gifted and I would like to express my profound gratitude to my internal advisor Dr Jayasankar Variyar for his support throughout my undergraduate studies.

I would like to express my profound gratitude to Dr. Pramod Kumar of Indian Institute of Science who was my external guide. I thank him for his continuous support and belief in the project during the times I was not confident about it. I would like to thank him for introducing me to the fascinating world of magnetohydrodynamics and its vast potential.

I am grateful to the members at www.cfd-online.com , in particular to Dr. Marcel Bachmann for his help when I was stuck with the code.

I would also like to express my thanks to the lab members of the Thermal Engineering Systems Lab for keeping the atmosphere light – Naunidh, Aditya, Ashutosh, Dhananjay, Bipin, Hitesh and Jyothsna mam.

I would also like to thank my friends at VIT-Chennai and the entire team of The Roadrunners (SAE BAJA India team) for all those memorable moments.

(To be signed by the student)
Reg. No. 10BME 1043

ABSTRACT

Electromagnetic Stirring (EMS) is a well know phenomena wherein Lorentz forces are used to create convection in the conducting fluids (liquid metals) without contaminating the fluid. EM forces are generated by passing phase displaced alternating currents through a set of fixed coils (stator). The traveling primary current field in the stator induces a magnetic field in the conductor (rotor) placed in the annulus of the stator. The induced magnetic field sets up a secondary opposing current in the rotor. This combination of opposing current along with the primary magnetic field (in the stator) together produces a net force in the rotor known a Lorentz force. If a liquid metal is placed in the annulus, the Lorentz forces cause the melt to convect. The convection in the melt alters the induced magnetic field in the rotor which has a net effect on the magnitude of Lorentz forces generated. Therefore a coupled solution of fluid flow magnetic field is necessary to capture the entire physics.

Simulation is considered an important and cost effective tool for industry research and development. In the present work, FLUENT commercial solver is used to solve the above problem. A separate user defined module (UDF) is written to solve for electromagnetic forces. The thesis work solves electromagnetic field problems for simple geometries and a close match between the analytical and computational results is observed. The thesis makes a small contribution to the existing state of the art by modeling phase displaced currents which can be used to design the stirrer.

In the future, the solidification and melting of a metal can be tracked by using the in-built Solidification module in FLUENT. Thus, the work done in this thesis serves as a foundation for designing a linear electromagnetic stirrer (LEMS).

.

LIST OF FIGURES

LIST OF TABLES

LIST OF SYMBOLS AND ABBREVIATIONS

$\nabla \cdot$	Divergence Operator	
$\nabla \times$	Curl Operator	
∇	Gradient Operator	
$\frac{\partial}{\partial t}$	Partial derivative	
E	Electric Field	V/m
D	Electric Displacement field	C//m^2
B	Magnetic Flux density	Wb/m^2 or T
H	Magnetic Field strength	A/m
μ	Magnetic Permeability	H/m
μ_0	Magnetic Permeability of free space	
μ_r	Relative Magnetic Permeability	
σ	Electrical Conductivity	S/m
$\boldsymbol{\varepsilon}$	Permittivity	F/m
ρ_e	Volumetric Charge Density	C/m^3
F	Lorentz force density	N/ m^3
v	Velocity of fluid	m/s
R	Electrical resistance	Ω
I	Electric Current	A
V	Electric scalar potential	V
A	Area of cross section of conductor	m^2
J	Current density	A/ m^2
ρ	Resistivity	S/m
L	length of conductor	m
A	Magnetic vector potential	V.s/m
MMF	Magneto-motive force	
EMF	Electromotive force	

TABLE OF CONTENTS

CHAPTER 1

INTRODUCTION

1.1 SCOPE

This thesis covers the design and evaluation of a linear stirrer suitable for manufacturing semi-solid aluminum alloys.

The design problem in such a stirrer has been traditionally focused on evaluation of electromagnetic fields for a given geometry, electrical excitation and frequency of excitation and relate the same to the magnetic field, induced eddy currents and mechanical forces taking the velocity of the molten metal to be negligible, thus ignoring the coupling between velocity and magnetic field.

1.2 METHODOLOGY

1. Understand the governing (Maxwell's) equations of electromagnetism and the general form of scalar transport equation.
1. Literature review of concepts of magnetohydrodynamics – which is the study of the combined effects of electric, magnetic and flow fields.
2. Literature review of advantages of electromagnetic stirring, governing equations and the existing literature.
3. Understand the concepts and syntax of implementing user defined functions in FLUENT and writing user defined scalar transport equation.
4. Validate the case of magnetic field of a circular current carrying coil by comparing the results obtained by implementing the code in FLUENT with that of the results obtained from the analytical solution and plotted in MATLAB.
5. Model the stirrer geometry in SOLIDWORKS.
6. Analysis of the Electromagnetic stirrer in ANSYS.
7. Validate the results by performing an experiment and measure the forces generated.
8. Correlation Study of simulation results, Engineering Calculation and Physical test Results.

1.3 EXPECTED OUTCOMES

1. Validation of electromagnetic field problems by implementing user defined functions in FLUENT.
2. Coupling of the velocity and the magnetic field will present a more improved model than the existing ones.
3. Ability to incorporate excitations other than sinusoidal waveforms.
4. Optimization of design.

1.4 OUTLINE OF THE THESIS

Chapter 1: A brief introduction of the problem is given along with the methodology and the expected outcomes.

Chapter 2: Maxwell's Equations for electromagnetics are introduced along with a brief introduction to magnetohydrodynamics which gives further insight into understanding the mechanism of stirring. A literature review regarding existing stirrer geometries is given. A brief introduction to implementing user defined functions in FLUENT is given.

Chapter 3: The analytical solution to the problem is introduced and its limitations are discussed. The use of Magnetic vector potential and Electric scalar potential to simplify Maxwell's equations is then discussed which lays the foundation for computational solution of the problem.

Chapter 4: The solution of electromagnetic field problems using the formulation mentioned in Chapter 3 is given. The typical geometries considered are an infinitely long cylindrical wire and an infinitely long square bar. In this formulation (A-V), the driving force is the potential difference across the ends of a conductor. The results are validated with the analytical solutions and the computational results are in good agreement with the analytical solution

Chapter 5: An alternate formulation to the one presented in Chapter 4 is discussed. The reason for developing the alternate formulation is discussed. In this formulation (A-J), current density is considered as the driving force. This formulation is then validated against the results from Chapter 4 and a close fit is obtained.

Chapter 6: The formulation discussed in Chapter 5 is then extended to validate electromagnetic field problems involving circular geometries – ring and solenoid. The current sheet concept is discussed. The solenoid is subjected to a grid refinement study and to constant, space varying, time varying and space and time varying currents.

Chapter 7: The development of Linear Electromagnetic Stirrer is discussed and details regarding the implementation of three phase currents in the stirrer are given. As a starting point, the height of the stirrer is divided into three parts with each part carrying one phase. The results are discussed which give us an insight into the generation and control of Lorentz forces inside the stirrer

Chapter 8: The scope of the thesis work is discussed along with the future possibilities.

CHAPTER 2

LITERATURE REVIEW

2.1 LITERATURE REVIEW

Electromagnetics application today spans a lot of fields. A common and popular application is in metallurgy. Applications include induction furnaces, electromagnetic pumps, electro- magnetic levitators etc. The main advantage of using electromagnetic fields in all these applications is the absence of any physical contact with the metal to be processed. The result is always a clean process. Over the years applications have grown from heating to shaping the metals. Modern metallurgical processes use magnetic fields to control the flow, shape and solidification of liquid metal.

Solidification describes the phenomenon of liquid transforming into solid as a result of a decrease in liquid temperature. It occurs in a wide range of industrial processes like casting and semi-conductor growth. Electromagnetic Stirring during solidification of metals leads to morphological changes in the microstructure. Electromagnetically stirred billets form the feedstock for the popular form of metal processing known as Semi Solid Forming which is now increasingly used in the automotive industry.

2.1.1 Solidification with stirring

When a metal alloy is cast, solidification begins with the formation of a thin layer of solid metal at the surface of the mold [1]. As the solidification front progresses into the ingot, the solidification front becomes unstable and forms dendrites throughout the remaining liquid. This partially solidified region is termed as mushy zone. The bulk of the ingot remains in the solid-liquid state for a substantial amount of time while heat is extracted till the liquid solidifies. During this time the dendrites undergo a coarsening process that determines their ultimate morphology as shown in Figure 2.1.

Dendrites - from the ancient Greek word for tree - are tiny branching structures. The size, shape and orientation of the dendrites have a major effect on the strength, ductility

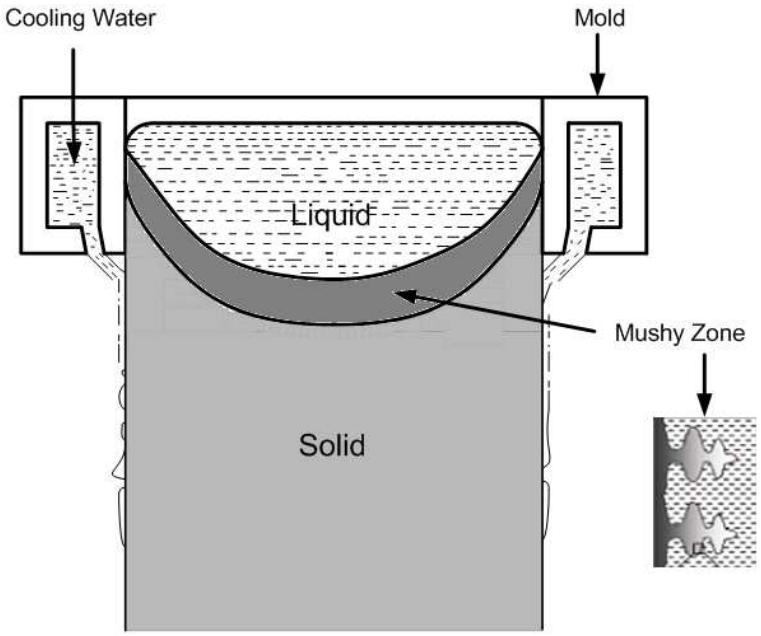

Figure2.1: Solidification during a casting process

And usefulness of an alloy. In many applications this dendritic microstructure is not desired as it results in poor mechanical properties. The dendritic structure is greatly affected by convection during the early effects of solidification. Enhancing the fluid flow by convection in the mushy zone is one of the means to suppress this dendritic growth [2]. Stirring is commonly used to obtain such vigorous convection in continuous castings. Stirring can be affected by

- using a mechanical device mechanical stirring
- Electromagnetic stirring.

The mechanical stirring is commonly effected by means of augers, impellers, or multi-paddle agitators mounted on a central rotating shaft. However, the mechanical agitation approach is characterized by several specific and serious drawbacks. It is primarily suited for batch, rather than continuous, production. Also, the erosion of these mechanical agitators which is immersed into a very aggressive medium, results in undesirable pollution of the melt. The above factors have made electromagnetic stirring a popular choice for stirring molten metals. The metallurgical effects of electromagnetic stirring have been described in [3], [4].

2.2 THE MAGNETOHYDRODYNAMIC PHENOMENON

Back in January 1832, Michael Faraday set up a rudimentary magnetohydrodynamic power generator. He placed two copper electrodes in the river Thames in London and measured a voltage between them. Although the demonstration was not fully successful, Faraday thus demonstrated that the motion of an electrically conducting fluid, here the salty water of river Thames, under the influence of a magnetic field, here the Earth's magnetic field induces an electric current.

A solid or liquid moving in a magnetic field experiences an emf. If the material is electrically conducting and a current path is available, currents ensue. Alternatively, currents may be induced by a varying magnetic field. There are two consequences:

(i) An induced magnetic field associated with these currents appears perturbing the original magnetic field.
(ii) An electromagnetic force due to the interaction of currents and field appears perturbing the original motion.
These are the two basic effects of Magnetohydrodynamics, the science of electrically conducting fluids under magnetic fields. It deals with the mutual interaction between the fluid velocity field and the electromagnetic field; the motion affects the magnetic field and magnetic field affects the motion.

Hartmann, in 1937, analytically solved the flow of a fluid between two stationary fixed parallel plates and a constant magnetic field applied in the perpendicular direction to fluid flow. This was the first major contribution to this field. Excellent introductory textbooks on Magnetohydrodynamics have been written by Davidson [5], Moffatt [6], Moreau [7] and Shercliff [8]. A review on electromagnetic stirring and the challenges have been summarized in [9], [10].

The equations for the calculation of the Lorentz force are mathematically represented below:

$$\frac{-\partial B}{\partial t} = \nabla x E \tag{2.1}$$

$$\boldsymbol{\nabla \times H = J} \tag{2.2}$$

$$\nabla \cdot \mathbf{H} = 0 \tag{2.3}$$

$$\mathbf{B} = \mu \mathbf{H} \tag{2.4}$$

$$\mathbf{J} = \sigma \left(\mathbf{E} + \mu \, \mathbf{v} \times \mathbf{H} \right) \tag{2.5}$$

The mechanical forces given by the vector cross products are as follows:

$$\mathbf{F} = \mathbf{J} \times \mathbf{B} \tag{2.6}$$

2.3 REVIEW OF ELECTROMAGNETIC STIRRER GEOMETRIES

In this section the magnetic field orientations and a coil configuration for basic stirrer geometries is briefly discussed. A cylindrical coordinate system for force field calculations is adopted due to axisymmetric nature of most stirrer geometries. The direction and magnitude of the Lorentz force, **F**, in the melt is governed by the following variables:

1) Induced current **J**
2) Induced magnetic field density **B**

The above two variables, **J** and **B**, in the metal follow the signature of the primary excitation current, **I**. The direction of **J** opposes the excitation current and the direction of **B** is normal to it. The direction of the excitation current, geometrical placement of the primary solenoid and location of the secondary conductor (molten metal) are the key parameters in the design of an electromagnetic stirrer. Depending on the requirement of force direction, the primary conductors are spatially arranged to obtain various field orientations in r,θ and z directions. The possible orientation of primary conductor and the resulting magnetic field directions are schematically represented in Figure 2.2

The three coil configurations shown in Figure 2.2 are commonly used in the design of electromagnetic stirrers. The stirrer configurations commonly used in liquid metal stirring are briefly described in the following subsections.

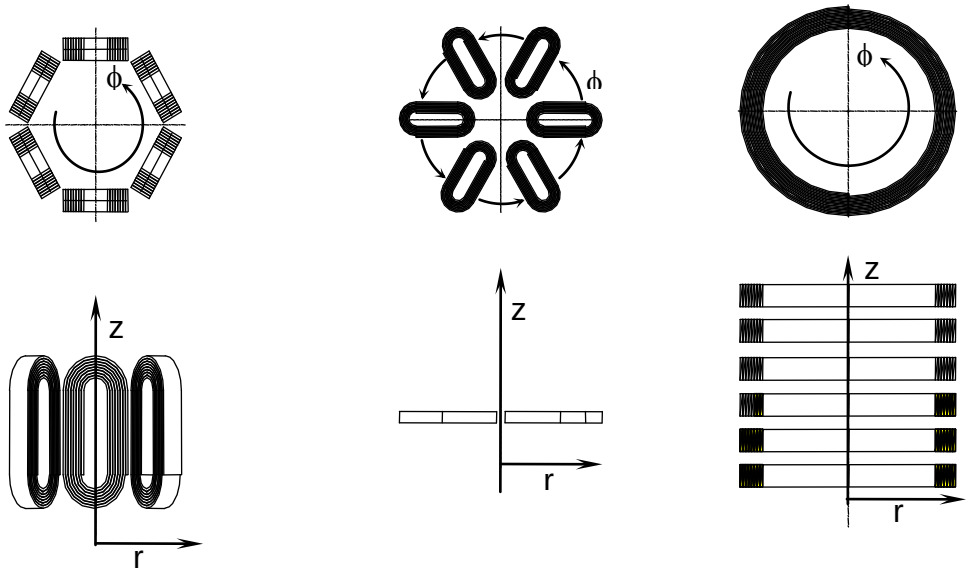

Coil configurations

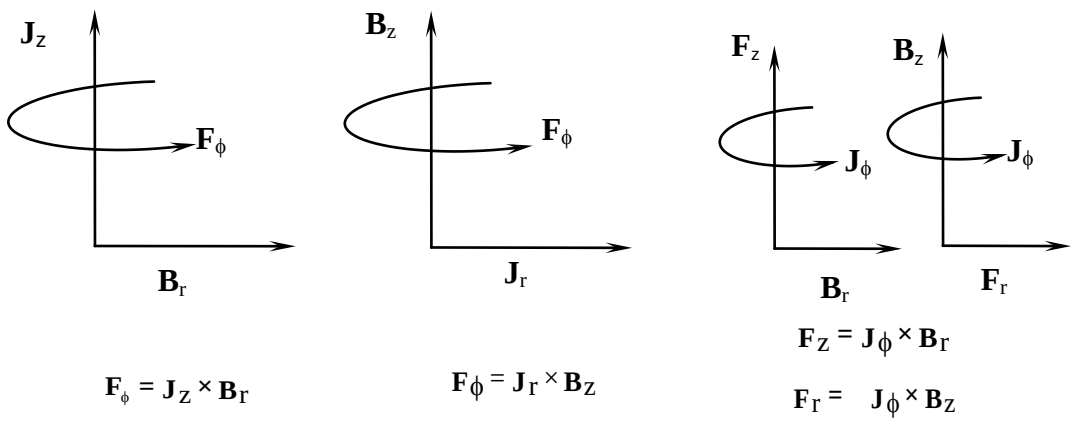

Field orientations and force directions

Rotary vortex stirrer	Rotary plate Stirrer	Linear axisymmetric stirrer
(a)	(b)	(c)

Figure 2.2 Common coil configurations in electromagnetic stirrer

a) Rotary vortex stirrer, b) Rotary plate stirrer, c) Linear axisymmetric stirrer

2.4 LINEAR AXISYMMETRIC STIRRER

Linear axisymmetric stirrers work on the same principle as a linear induction motor. The travelling magnetic field along the axis of the stirrer is responsible for generating axial forces necessary for creating forced convection in the vertical direction. Convection in the vertical direction is ideal for shearing dendrites at the solid/liquid interface for the case of

bottom cooled mould. These stirrers are very effective where the aspect ratio of the mould is high (i.e. L/D >>1 where L is the length of stirrer and D is diameter), as in the case of thixo-casting or rheocasting. The direction of force field can be reversed by changing the phase sequence of primary current to overcome gravity induced effects. Also, the radial penetration of the force can be effectively controlled by changing the excitation frequency of the primary current. This ensures good radial mixing in addition to uniform mixing throughout the height of the mould. A linear electromagnetic stirrer is shown in Figure 2.3.

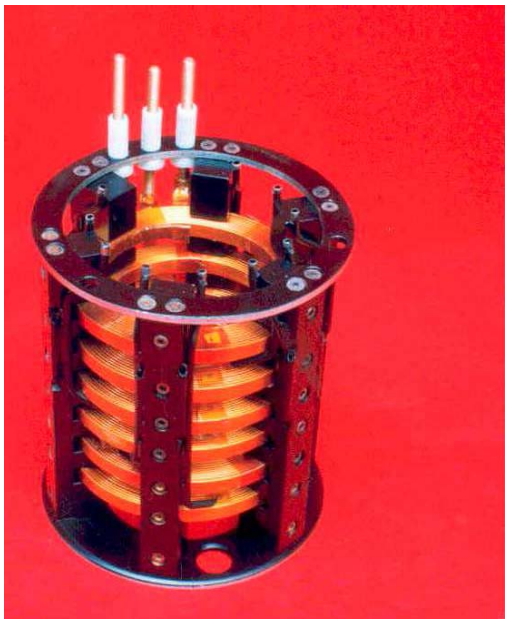

Figure 2.3 Coil Assembly

Extensive research has been carried out on Rotary Electromagnetic Stirrer [11], [12]. As for Linear Electromagnetic stirrers, the research done by V.Ramanaraynan, P.Dutta [13], [14] serves as the basis for conducting further investigation. The idea of current sheet is used to obtain the induced magnetic field. The three phase coils through which current is supplied to the LEMS coils are assumed to be equivalent to a current sheet. Using this idea of equivalence, the magnetic field induced and thus the induced currents and Lorentz forces are found.

The analytical model for the design of stirrer described by Marr [9], has the limitation that it decouples the electromagnetic and momentum equations.

2.5 INTRODUCTION TO FLUENT COMMERCIAL CODE

ANSYS INC offers a wide range of inbuilt modules by the name of ANSYS to solve problems related structural, mechanical and electromagnetism. FLUENT.INC. is now completely owned by ANSYS and it is a commercial solver written in C language and integrated into ANSYS. FLUENT is one of the most robust solvers available to solve flow and heat transfer problems with an ability to write user defined functions to suit problem conditions. Different solution schemes are available for solving flow and heat transfer problems. [15]

2.5.1 User Defined Functions in FLUENT

The need of a User Defined Function (UDF) arises because:

1. The codes solved in FLUENT cannot anticipate all needs.
2. New physical models can be developed in a user friendly environment.
3. Large number of problems can be addressed with same implementation.

While solving equations FLUENT takes into account certain assumptions. To include source terms or generalize the equation or modify the equation as needed a UDF needs to be written. Figure 2.4 shows the entities in FLUENT. A collection of entities is called a zone or thread. Domain comprises of all the threads or different zones. An advantage of writing a UDF is that their syntax is derived from C language. As an example, to give variable inlet velocity, the steps are as follows [16]:

1. Identify the inlet faces.
2. Loop over them
3. Find the centroid of the face
4. Apply a velocity profile

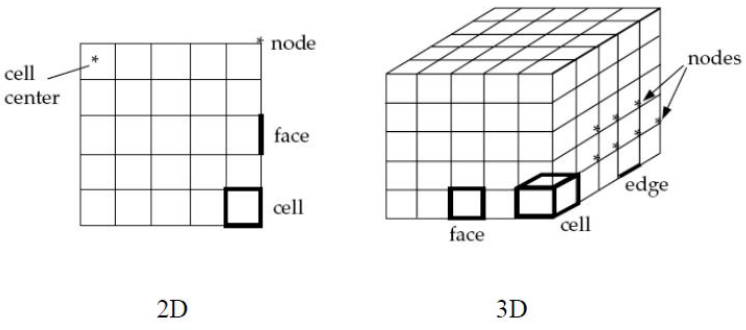

Figure 2.4: Entities in FLUENT

A UDF must be linked to the main code. This can be done in two ways:

1. **Interpreted UDF:**

The code is executed on a line by line basis.

a. It does not need a separate compiler.
b. It slows down execution.
c. The scope is limited as Structure references cannot be implemented.

2. **Compiled UDF:**

a. A library of UDF is compiled and linked to the main code. Overcomes all the shortcomings listed above.

The general solution procedure and the sequence of calling the UDF for Pressure based segregated solver is shown in Figure 2.5.The User defined Scalar Transport equation is solved in the general form as:

$$\frac{\partial \rho \emptyset}{\partial t} + \nabla\left(\rho \boldsymbol{u} \emptyset - (\tau \nabla \emptyset)\right) = S_{\emptyset} \qquad (2.7)$$

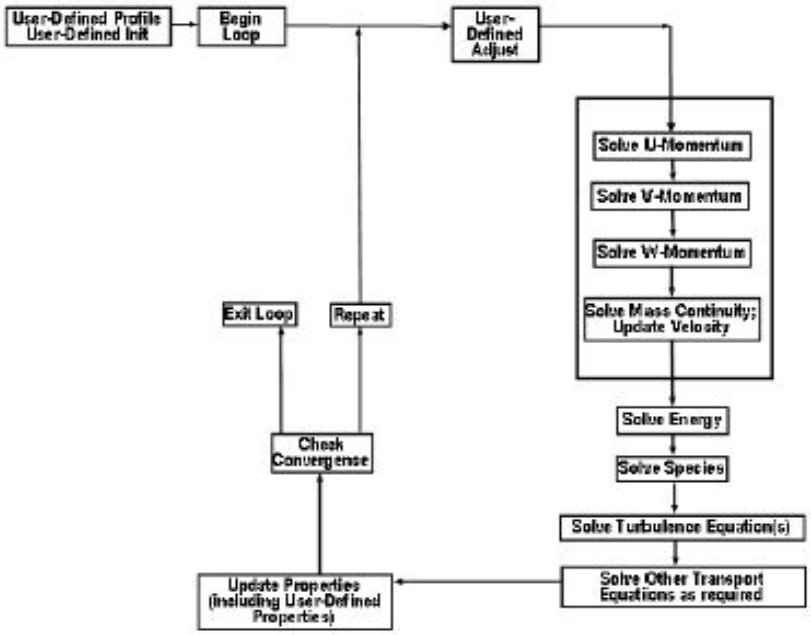

Figure 2.5: Solution Procedure for Pressure Based solver

CHAPTER 3

POTENTIAL FORMULATION FOR ELECTROMAGNETIC FIELD PROBLEMS

3.1 INTRODUCTION

In the first and second chapter, a detailed description regarding the working and types of electromagnetic stirrer was done. This was accompanied by a discussion of Magnetohydrodynamics phenomena and the governing equations that are used to model electromagnetic stirring.

In this chapter, a detailed discussion regarding the boundary conditions for Maxwell's equations and potential formulation to simplify Maxwell's equations will be done. Subsequently, this formulation was used to validate the magnetic field around a current carrying conductor by implementing user defined functions in FLUENT commercial solver.

3.2 EQUATIONS DEFINING ELECTROMAGNETIC PROBLEM

As discussed in the second chapter, the Maxwell's equations are described below:

$$\text{Faraday's Law: } \nabla \times \vec{E} = -\frac{\partial \vec{B}}{\partial t} \tag{3.1}$$

$$\text{Ampere's Law: } \nabla \times \vec{H} = \vec{j} + \frac{\partial \vec{D}}{\partial t} \tag{3.2}$$

$$\text{Gauss Law (electric): } \nabla \cdot \vec{D} = \rho_e \tag{3.3}$$

$$\text{Gauss Law (magnetic): } \nabla \cdot \vec{B} = 0 \tag{3.4}$$

The general form of Ohm's Law is given by:

$$\mathbf{J} = \sigma\left(\mathbf{E} + (\mathbf{v} \times \mathbf{B})\right) \tag{3.5}$$

The mechanical forces given by the vector cross products are as follows:

$$\mathbf{F} = \mathbf{J} \times \mathbf{B} \tag{3.6}$$

The constitutive relations are:

$$\mathbf{B} = \mu\,\mathbf{H} \tag{3.7}$$

$$D = \varepsilon E \tag{3.8}$$

A typical structure of an eddy-current problem with conducting and non-conducting regions is shown in Figure.3.1. The boundaries of the conducting region W_1 and the non-conducting region W_2 are denoted by G_1 and G_2, respectively. The interface between these two regions is denoted by G_{12} and is a part of G_1 and G_2. Coils carrying known source current densities $\boldsymbol{J}$c are included in the non-conducting region W_2. The arrows illustrate the flow of a magnetic field. These arrows are used to distinguish between the two parts G_H and G_B of the outer boundary where different conditions apply. Those parts of G_1 and G_2 which belong to GH are denoted by GH_1 and GH_2, respectively. Similarly, those parts of G_1 and G_2 which belong to GB are denoted by GB_1 and GB_2, respectively. At the interface G_{12}, Maxwell's equations imply continuity conditions on the normal component of the magnetic flux density and on the tangential component of the magnetic field intensity,

$$\boldsymbol{B_1} \times \boldsymbol{n}_1 + \boldsymbol{B_2} \times \boldsymbol{n_2} = 0 \tag{3.9}$$

$$\boldsymbol{H_1} \cdot \boldsymbol{n}_1 + \boldsymbol{H_2} \cdot \boldsymbol{n_2} = 0 \tag{3.10}$$

Where $\boldsymbol{n}_1$ and $\boldsymbol{n}_2$ are the unit normal vectors directed outward from the conducting and the non-conducting regions, respectively

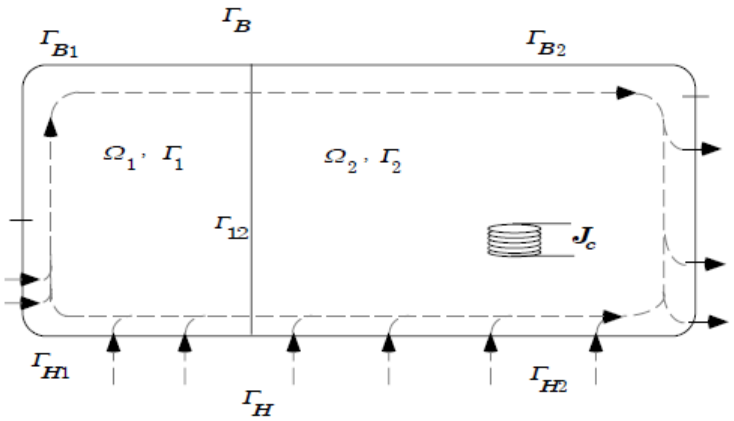

Figure 3.1: Typical structure of an eddy current problem with conducting and non-conducting regions

On the outer boundary, three conditions are imposed: the tangential component of the magnetic field intensity is zero on G_H

$$\boldsymbol{H} \times \boldsymbol{n} = \boldsymbol{0} \quad (3.11)$$

The normal component of the magnetic flux density is zero on G_B

$$\boldsymbol{B} \cdot \boldsymbol{n} = 0 \quad (3.12)$$

and the normal component of the current density is zero on G_1

$$\boldsymbol{J} \cdot \boldsymbol{n}_1 = 0 \quad (3.13)$$

Where $\boldsymbol{n}$ is the unit normal vector directed outward from the region in question. The boundary and interface conditions are assumed to be homogeneous for the sake of simplicity. A detailed derivation of the boundary conditions is presented in [17].

3. 3 POTENTIALS DESCRIBING THE ELECTROMAGNETIC FIELD

The electromagnetic field variables $\boldsymbol{H}$ and $\boldsymbol{E}$ can be solved directly, but it is often found to be advantageous to use potentials describing the field. If $\boldsymbol{H}$ or potentials describing $\boldsymbol{H}$ are used as unknowns, the formulations are called magnetic formulations.

According to the principles of Vector calculus, $\nabla \cdot \left(\nabla x \vec{A}\right) = 0$

Hence, we define, Magnetic vector potential A as

$$\vec{B} = \nabla x \vec{A} \quad (3.14)$$

Substituting (3.14) in (3.1),

$$\nabla x \left(E + \frac{d\vec{A}}{dt}\right) = 0 \quad (3.15)$$

Defining a electric scalar potential V as,

$$\nabla \mathrm{V} = -\left(E + \frac{d\vec{A}}{dt}\right) \quad (3.16)$$

This formulation is referred as the A-V formulation

The following assumptions are taken due to the nature of the problem:

1. Electro-neutrality

Using the equation for conservation of charge,

$$\frac{\partial q_e}{\partial t} + \nabla \cdot \vec{j} = 0 \quad (3.17)$$

With the assumption that each volume element is electrically neutral at macroscopic scale (total electric charge is zero), results in,

$$\nabla \cdot \vec{j} = 0 \quad (3.18)$$

2. Quasi steady electromagnetic phenomena

Considering Ampere's Law (3.2), if the dimension of eddy current regions is small compared with the effect of prescribed fields, the displacement current, $\frac{\partial D}{\partial t}$, can be neglected.

Thus Ampere's Law reduces to:

$$\nabla \times \vec{H} = \vec{j} \tag{3.19}$$

Taking divergence of (3.5), using (3.16) neglecting the induction term **(v × *B*)**

$$\nabla \cdot j = \nabla \cdot (\sigma E) = -\nabla \cdot \sigma \left(\nabla \mathrm{V} + \frac{\partial A}{\partial t}\right) = 0 \tag{3.20}$$

For magnetostatic cases [18] or for an axisymmetric AC arc [19], $\frac{\partial A}{\partial t}$ is neglected. Thus (3.20) essentially states that current is divergence free and charge is conserved.

This leads to $\nabla \cdot \sigma(\nabla \mathrm{V}) = 0$ (3.21)

When the induction term is included in Ohm's Law, (3.21) becomes

$$\nabla \cdot \sigma(\nabla \mathrm{V}) = -\nabla \cdot (\sigma \vec{v} \times \vec{B}) \tag{3.22}$$

this is numerically more tedious to solve.

For the magnetostatic case or when velocities of fluid are low, (3.20) is used. Magnetic Reynolds number ($Re_m = \sigma \mu U_0 L$) is used to determine if the induction term is neglected or not.

Considering (3.19),

$$\nabla \times \vec{B} = \nabla \times (\nabla \times \vec{A}) = \mu \vec{j}$$

$$\nabla \times \left(\nabla \times \vec{A}\right) = \nabla \cdot \left(\nabla \cdot \vec{A}\right) - \nabla^2 \vec{\mathrm{A}} = \mu \vec{j}$$

Using Coulomb Gauge Condition [18] , [19],$\nabla \cdot \vec{A} = 0$,

$$\nabla^2 \vec{\mathrm{A}} = -\mu \vec{\mathrm{j}} \tag{3.23}$$

3.3.1 Simplified equation set

$$\nabla \cdot \sigma(\nabla \mathrm{V}) = 0 \tag{3.24}$$

$$\vec{j} = -\sigma \nabla V \tag{3.25}$$

$$\nabla^2 \vec{\mathrm{A}} = -\mu \vec{\mathrm{j}} \tag{3.26}$$

$$\vec{B} = \nabla x \vec{A} \tag{3.27}$$

3.4 FORCE FIELD CALCULATIONS IN THE METAL

When an electrical conductor such as molten metal is introduced in the field space, the induced currents in the metal oppose the primary excitation current as shown in Figure 3.2. This alters the magnetic field intensity **H** in the field space. The field equations in such a case are defined by the following equation [20]:

$$\frac{\partial^2 H_z}{\partial r^2} + \frac{1}{r}\frac{\partial H_z}{\partial r} - \mu\sigma\frac{\partial H_z}{\partial t} = 0 \qquad (3.28)$$

Where, r is the radial distance (m), σ is electrical conductivity of metal (S/m) and μ is the magnetic permeability of the material (H/m).

The above equation is valid under the following assumptions:

1) The stirrer is infinitely long in the *z* direction (i.e. L>>R). In such cases, the travelling field is completely axial and is defined as

$$H_Z(z,t) = H_o \sin\left(\omega t - \frac{2\pi Z}{L}\right) \qquad (3.29)$$

2) The electromagnetic equations are decoupled from the fluid flow momentum equations. In other words, the current density **J** in the molten metal is not a function of melt velocity. From eqn. (3.2), **J** is now calculated using eq. 3.2

$$\mathbf{J} = \nabla \times \mathbf{H}$$

3) The end effects and flux leakage due to the presence of air gap between the primary coils and the metal core are ignored.

4) The entire magnetic flux generated by the primary coils is concentrated in the core of the LEMS where the metal is placed.

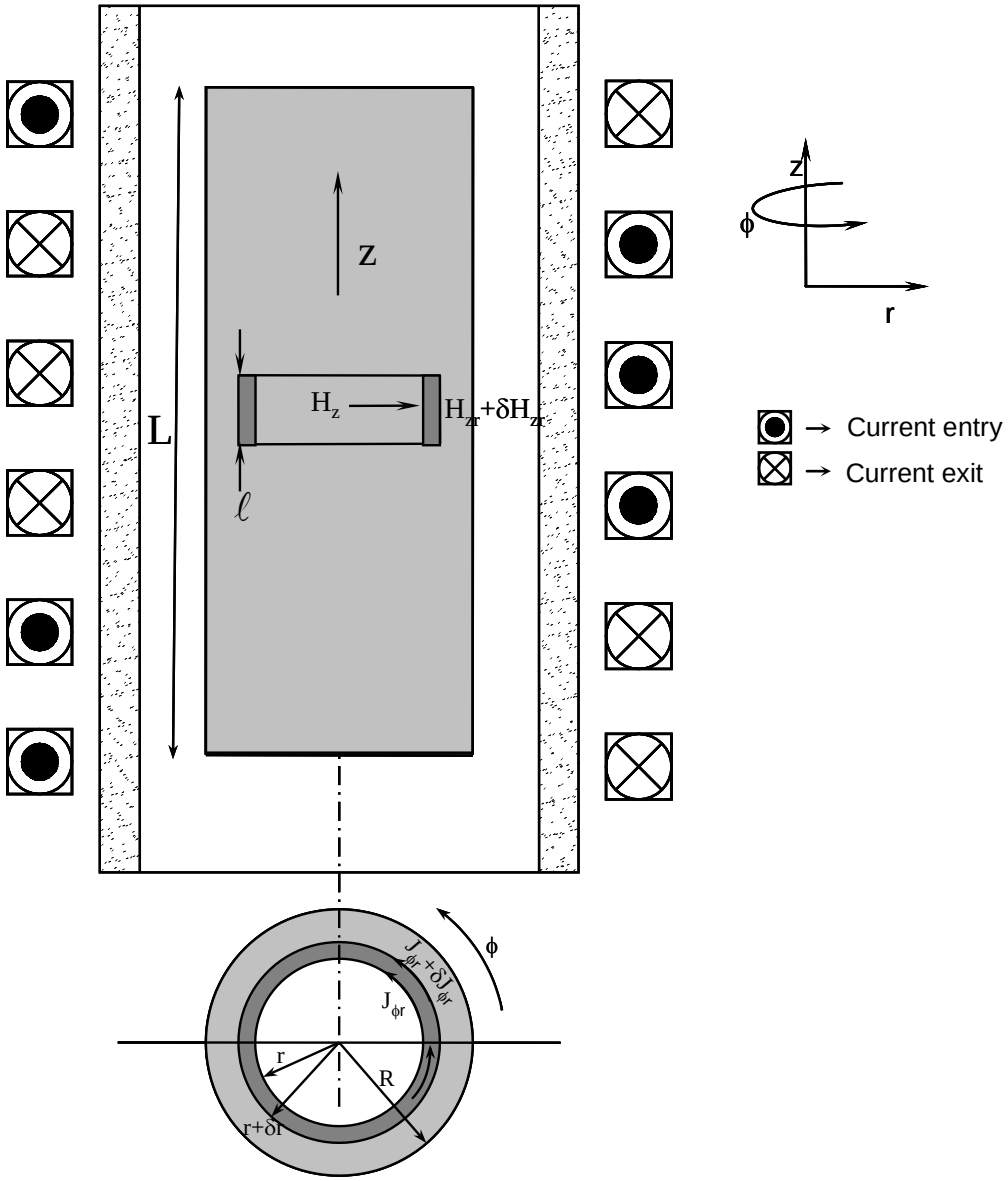

Figure 3.2: Field formulation for J (A/m^2) in the metal.

Using $H_z = H_o\, e^{-j\left(\omega t - \frac{2\pi Z}{L}\right)}$ for the sinusoidally excited current, the above governing equation (3.29) takes the form of a standard Bessel's function of order zero.

$$\frac{\partial H_z}{\partial r^2} + \frac{1}{r}\frac{\partial H_z}{\partial r} + j\mu\sigma\omega H_z = 0 \qquad (3.30)$$

The solution of the above equation is given by

$$H_z(z,r,t) = \left(\frac{\text{ber}(kr) + \text{bei}(kr)}{\text{ber}(kR) + \text{bei}(kR)}\right) H_o \sin\left(\omega t - \frac{2\pi z}{L}\right) \qquad (3.31)$$

Where ber(kr) and bei(kr) are the real and imaginary parts of the Bessel's function, given by the following expressions:

$$\text{ber}(kr) = 1 - \frac{\left(kr/2\right)^4}{2!} + \frac{\left(kr/2\right)^8}{4!} - \ldots\ldots \qquad (3.32)$$

$$\text{bei}(kr) = \frac{\left(kr/2\right)^2}{(1!)^2} - \frac{\left(kr/2\right)^6}{(3!)^2} + \frac{\left(kr/2\right)^{10}}{(5!)^2} \ldots\ldots \qquad (3.33)$$

$$\text{ber}(kR) = 1 - \frac{\left(kR/2\right)^4}{2!} + \frac{\left(kR/2\right)^8}{4!} - \ldots\ldots \qquad (3.34)$$

$$\text{bei}(kR) = \frac{\left(kR/2\right)^2}{(1!)^2} - \frac{\left(kR/2\right)^6}{(3!)^2} + \frac{\left(kR/2\right)^{10}}{(5!)^2} \ldots\ldots \qquad (3.35)$$

where k is a skin depth parameter defined as,

$$k = \sqrt{\mu\sigma\omega} \qquad (3.36)$$

The solution of the above equation is used to obtain the eddy current distribution in the metal defined by

$$J_\phi(r) = \frac{\partial H_z}{\partial r} \qquad (3.37)$$

The eddy current distribution in the metal is given by

$$J_\phi(z,r,t) = \sqrt{\frac{\text{ber}'(kr)^2 + \text{bei}'(kr)^2}{\text{ber}(kR)^2 + \text{bei}(kR)^2}}\ H_o \sin\left(\omega t - \frac{2\pi Z}{L} - \theta_J(r)\right) \qquad (3.38)$$

where $\text{ber}'(kr)$ and $\text{bei}'(kr)$ are the first derivatives obtaining by differentiating equations. (3.32) and (3.33) and $\theta_J(r)$ represent the leading or lagging phase angle obtained from field plots.

Using the above expressions for the current distribution $\mathbf{J}_\phi$ and the induced magnetic flux density, $\mathbf{B}_r$ and $\mathbf{B}_z$, in the radial and axial directions, respectively, the force field distribution in the metal is given by the following equations.

$$\mathbf{F}_z = \mathbf{J}_\phi \times \mathbf{B}_r \qquad (3.39)$$

$$\left|\mathbf{F}_z\right| = \mu_o J_o H_o \frac{r^2}{R^2}\left\{\frac{1}{2} - \frac{\cos 2\left[\omega t - \frac{(2\pi z)}{L}\right]}{2}\right\} \qquad (3.40)$$

and,

$$\mathbf{F}_r = \mathbf{J}_\phi \times \mathbf{B}_r \tag{3.41}$$

$$|\mathbf{F}_r| = -\mu_o J_o H_o \frac{r}{R}\left\{\frac{\sin 2\left[\omega t - \frac{(2\pi z)}{L}\right]}{2}\right\} \tag{3.42}$$

The magnetic flux density **B** in the above equations is calculated using eqn. (3.2) From eqns. (3.40) and (3.41), we note the following,

1) The axial and radial force densities are proportional to the square of the radius and radius, respectively.

2) The radial force averaged in space and time, is zero.

3) The axial force, when averaged in space or time, is in the direction of phase sequence.

The average axial force is given by:

$$F_{zavrg} = \int_0^R (F_z 2\pi L r)dr \tag{3.43}$$

$$F_z(z,r,t) = \frac{\mu_o \pi L J_o H_o R^2}{4} \tag{3.44}$$

In a LEMS, it is the axial force (F_z) which is responsible for bulk motion in the liquid. Since the net average radial force is zero, it does not directly play a role in the fluid motion. The radial force, at most, would create a pressure field around the melt.

CHAPTER 4

VALIDATION OF ELECTROMAGNETIC FIELD PROBLEMS USING A-V FORMULATION

4.1 INTROUDCTION

4.2 VALIDATION OF FLUENT SIMULATIONS ON A 2D AXISYMMETRIC GEOMETRY

4.2.1 Geometric properties for 2D Axisymmetric Geometry

The thesis by Zhe Huang [18] is taken as the reference for validation problems because the thesis validates the result obtained by OpenFoam simulations with that of COMSOL simulations along with then analytical result. Thus a strong agreement with these results would validate the code solved in FLUENT.

The 2D axisymmetric geometry is shown in Figure 4.1. It comprises of a conductor of radius **r** m surrounded by an air box of radius **R** m, both have the same length **L** m. The dimensions are given in Table 4.1.

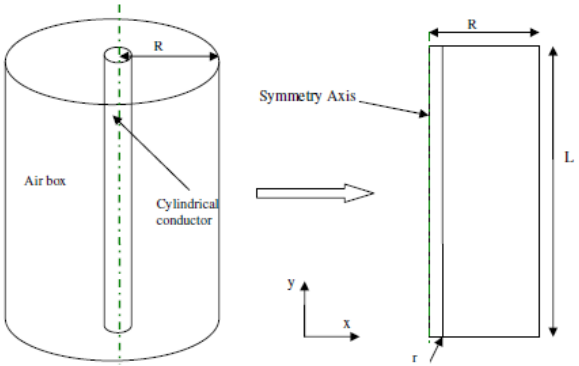

Figure 4.1: Geometry conversion from 3D to 2D axisymmetric

Table 4.1: Geometric data for 2D Axisymmetric geometry

r (inner radius) m	R (outer radius) m	L (Length) m
0.2	2	6

4.2.2 Mesh Generation in ANSYS

FLUENT requires that X Axis be the axis of symmetry [16]. The Geometry along with the Named Selections is shown in Figure 4.2. The Mesh comprises of 50 Cells in X direction (axial direction) and 68 Cells in Y direction (radial).

Figure 4.2: 2D Axisymmetric Geometry with Named Selctions

4.2.3 Boundary Conditions and Initial Values

As shown in Table 4.2 and Table 4.3, potential difference between two ends is the driving force.

Table 4.2: Material properties for 2D Axisymmetric Geometry

Material	μ (H/m)	Electric Potential (V)	Electrical Conductivity (S/m)
Copper	1.26e-6	High:670; Low:0	2700
Air	1.26e-6	0	1e-5

Table 4.3: Boundary conditions for 2D Axisymmetric Geometry

Named Selection	A(V.s/m)	V (V)
Conductor_up	Zero normal gradient	670
Conductor_down	Zero normal gradient	0
Up	Zero normal gradient	Zero normal gradient
Down	Zero normal gradient	Zero normal gradient
Far_walls	Zero value	Zero normal gradient
Axis	Axis	Axis

Zero normal gradient (normal implies the direction of outward normal vector of the surface under consideration) corresponds to Neumann boundary condition and Zero value corresponds to Dirichlet boundary condition. For Axis no boundary conditions are needed [16].

The Magnetic vector potential has two components – $\mathbf{A_z}$ and $\mathbf{A_r}$. Thus there are 2 UDS for A and 1 for electric scalar potential **V.**

Table 4.4 describes the conversion of the equations corresponding to the **A-V** formulation into user defined scalar transport equations required by FLUENT solver according to equation (2.7).

Table 4.4: Equations casted into UDS form

Scalar	Flux term coefficient	Diffusivity	Source Term
Az	0	1	μJz
Ar	0	1	μJr
V	0	σ	0

4.2.4 Results

The resulting magnetic field plot is shown in Figure 4.3 and compared with the analytical solution.

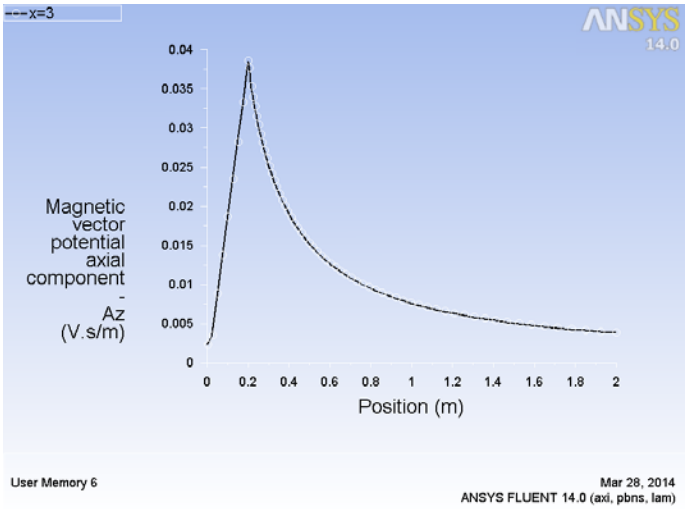

Figure 4.3: Line plot of Magnetic flux density at x=3 with the radial distance

The line plot of magnetic field inside the conductor is shown in Figure 4.4.

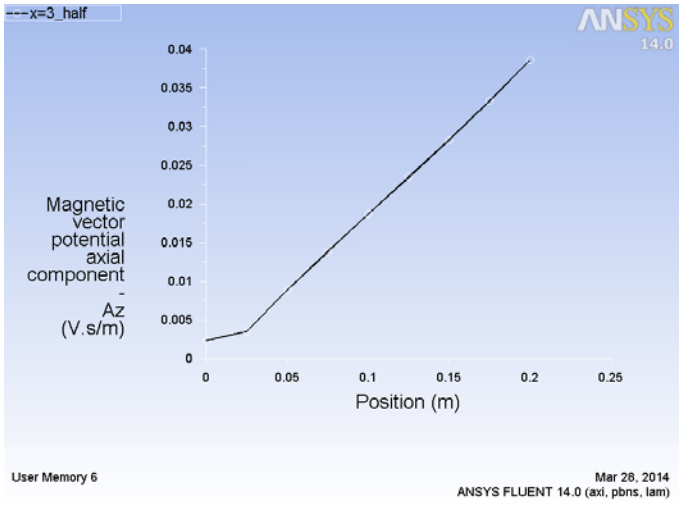

Figure 4.4: Line plot of Magnetic flux density inside the conductor

The line plot of analytic and numerical solution is shown in Figure 4.5. The maximum error is 1.45% which occurs at the singularity point where conductivity changes at r = 0.2m (highlighted by the data cursor).

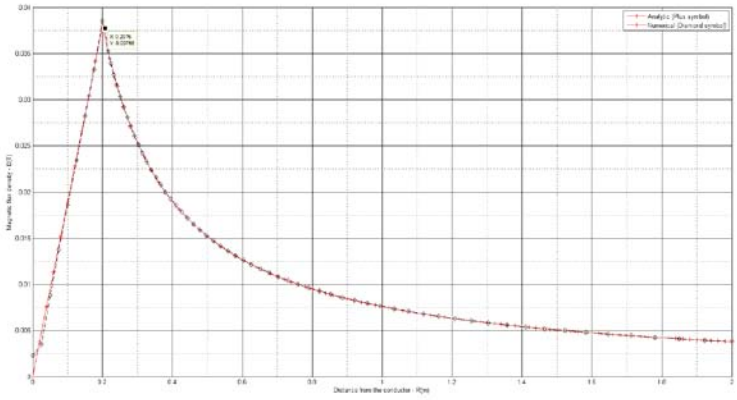

Figure 4.5: Comparison of Line plot of Magnetic flux density with analytical results

The line plot of axial component of magnetic vector potential is shown in Figure 4.6.

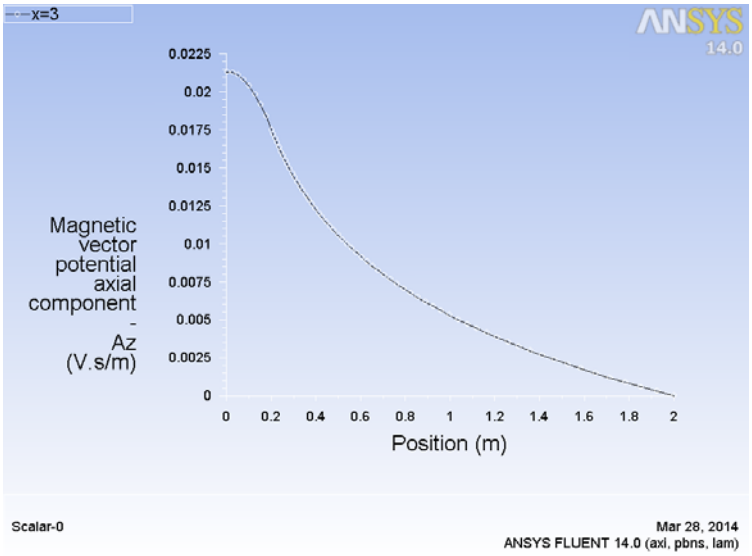

Figure 4.6: Line plot of A_z along radius

4.3 VALIDATION OF FLUENT SIMULATIONS ON A 3D SQUARE BAR

4.3.1 Geometric properties

The calculated domain is a cuboid copper wire surrounded by a cuboid air box in3 dimensions. The geometry data in 3D is given in Table 4.5 and Figure 4.7 shows the problem region. High voltage and low voltage are applied to the two ends of the copper bar separately.

Table 4.5: Geometric properties of bar

	x(m)	y(m)	z(m)
Conductor	0.4	0.4	6
Air box	44	4	6

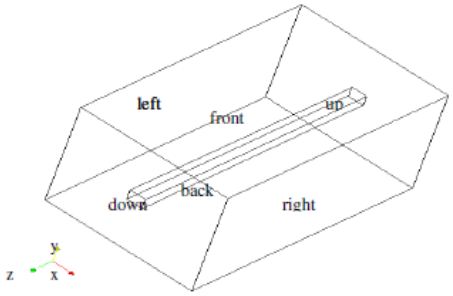

Figure 4.7: Geometry of single bar case

4.3.2 Mesh Generation and Boundary Conditions

A $20 \times 20 \times 30$ hex mesh is used initially which is refined gradually to $50 \times 50 \times 60$

The material properties and boundary conditions are shown in Table 4.6

Table 4.6: Boundary Conditions for Copper bar

Boundary	A(V.s/m)	V (V)
Conductor_up	Zero normal gradient	670
Conductor_down	Zero normal gradient	0
Up	Zero normal gradient	Zero normal gradient
Down	Zero normal gradient	Zero normal gradient
Far_walls	Zero value	Zero normal gradient
Axis	Axis	Axis

4.3.3 Results

The line plot of magnetic field at y, z =0 along x is shown in Figure 4.8. The symmetry of the magnetic field can be observed.

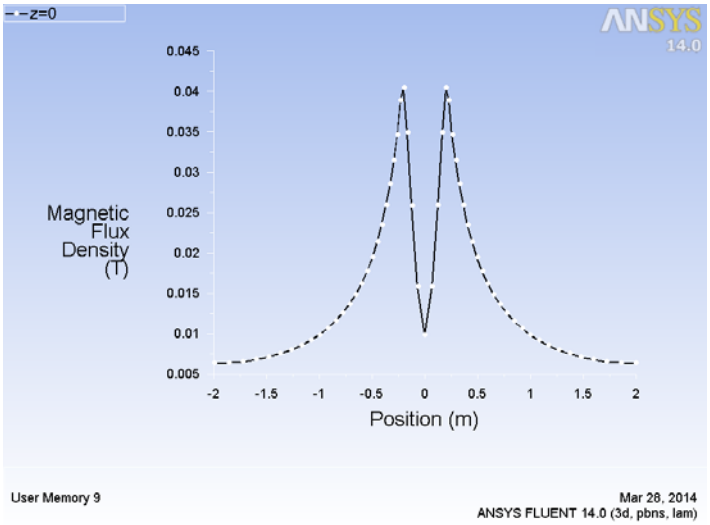

Figure 4.8: Line plot of Magnetic flux density along x (y =0, z=0)

The magnetic field inside the conductor is shown in Figure 4.8. Figure 4.8 and Figure 4.9 are similar to Figure 4.3 and Figure 4.4 respectively. They agree in principle that magnetic flux density is directly proportional to the radius inside the conductor and inversely proportional to the radius outside the conductor.

However, one thing that should be noted is that at r=0 from analytical solution, the magnetic flux density should be zero, however there remains some residual error at r=0 (of the order of 1%). The maximum error between the results computed in OpenFoam from [18] and the computed result of magnetic flux density is 1.45% the interface between conductor and air box.

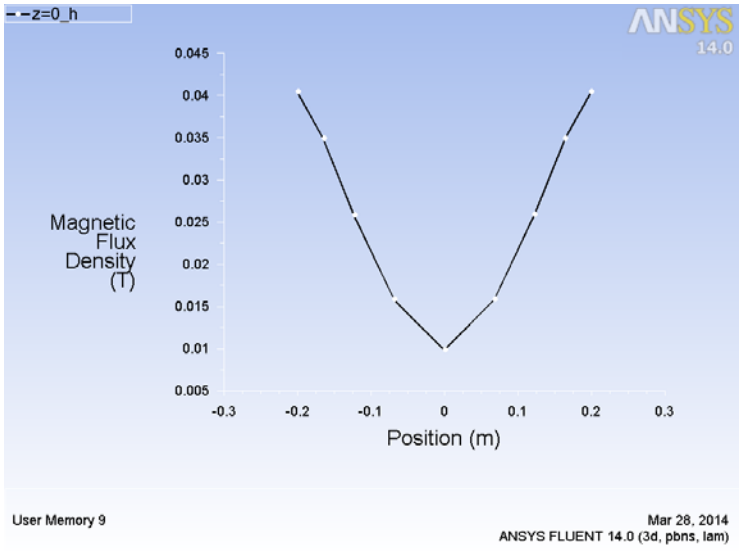

Figure 4.9: Line plot of Magnetic flux density inside the conductor along x (y =0, z=0)

The line plot of current density magnitude is shown in Figure 4.10. It can be observed that there are four points of singularity at the four vertices of the conductor which results in the erroneous jump of current density magnitude. This problem can be alleviated by making giving a fillet to the four vertices so that no sharp edges remain.

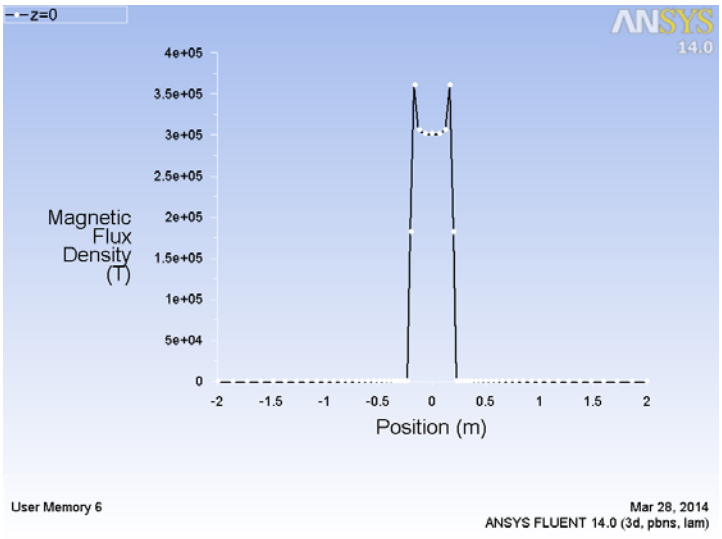

Figure 4.10: Line plot of current density magnitude along x (y =0, z=0)

The contour plot of Magnetic flux density and magnitude of magnetic vector potential are shown in Figure 4.11 and Figure 4.12 respectively.

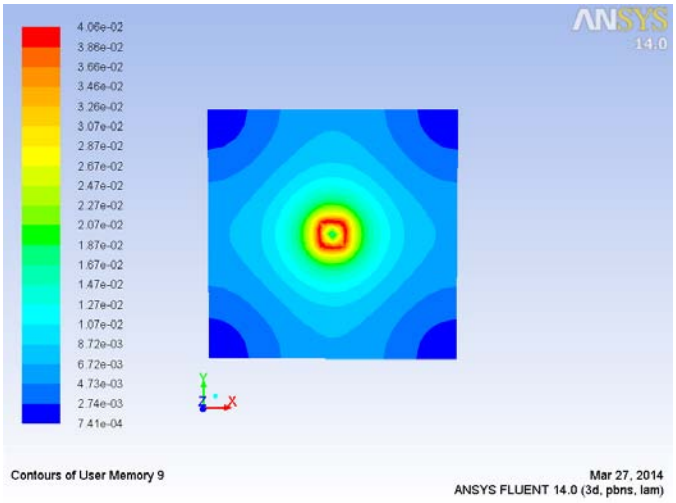

Figure 4.11: Contour plot of Magnetic flux density at z=0

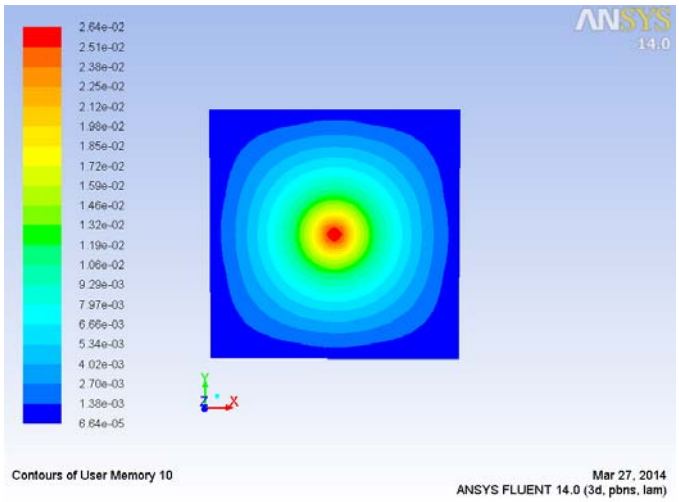

Figure 4.12: Contour plot of magnitude of Magnetic vector potential density at z=0

CHAPTER 5

VALIDATION OF ELECTROMAGNETIC FIELD PROBLEMS USING A-J FORMULATION

5.1 INTRODUCTION

In Chapter 4, the validation of the code was done for an infinitely long circular current carrying conductor, infinitely long current carrying square bar by finding the magnetic field and validating it against [18]. In the aforementioned validation cases, potential difference was the driving force. To find the magnetic field around a closed current carrying coil, it is necessary to specify the current density instead of the potential difference due to the closed nature of the current carrying conductor. In this chapter the formulation using current density will be described and this code will be validated against the results from Chapter 4.

5.2 FORMULATION INVOLVING CURRENT DENSITY (A- J formulation)

Considering the simplified equation set (3.3.1) from Chapter 3 as the starting point, this is also known as the A-V formulation,

$$\nabla \cdot \sigma(\nabla V) = 0 \quad (5.1)$$

$$\vec{j} = -\sigma \nabla V \quad (5.2)$$

$$\nabla^2 \vec{A} = -\mu \vec{j} \quad (5.3)$$

$$\vec{B} = \nabla x \vec{A} \quad (5.4)$$

It can be seen that the potential difference V is the driving force which creates the primary excitation current. If the current density J is known then equations (5.1) and (5.2) become redundant and the formulation involving current density, also known as the A-J formulation can be described as,

$$\nabla^2 \vec{A} = -\mu \vec{j} \quad (5.5)$$

$$\vec{B} = \nabla x \vec{A} \quad (5.6)$$

The **A-J formulation** is computationally less expensive to solve because of fewer

equations. The equations are casted into the form of User Defined Scalar transport equation as shown in Table 5.1

Table 5.1: Equations casted into UDS form

Scalar	Flux term coefficient	Diffusivity	Source Term
Ax	0	1	μJx
Ay	0	1	μJy
Az	0	1	μJz

5.3 IMPLEMENTATION AND VALIDATION

The equations shown in Table 5.1 are the equations (5.5), (5.6) casted in the form of user defined scalar transport equations (UDS) required by FLUENT.
The equivalent current density corresponding to the voltage applied is calculated using the following relations:

$$R = \frac{\rho L}{A} = \frac{L}{\sigma A} \tag{5.7}$$

$$I = \frac{V}{R} \tag{5.8}$$

The current density J can be computed using,

$$J = \frac{I}{A} \tag{5.9}$$

The equivalent current density corresponding to the given voltage is computed from (5.3), (5.4), and (5.5) which comes out to be 301500 A/m^2. The implementation is the same as described in Chapter 4.

5.4 VALIDATION OF FLUENT SIMULATIONS ON A 2D AXISYMMETRIC GEOMETRY

The Geometric properties, material properties and mesh generation have been described in Chapter 4. The boundary conditions are the same as shown in Table 4.3 except that since potential is not being solved, no boundary conditions need to be specified.

5.4.1 Results

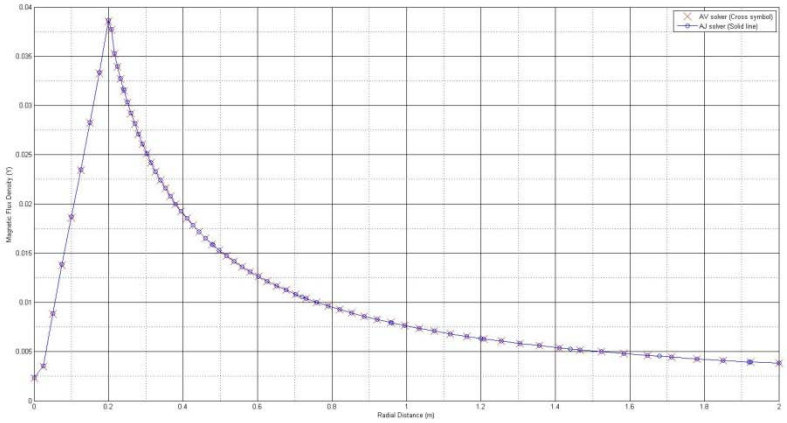

Figure 5.1: Comparison of variation of magnetic flux density along the radius computed using A-V and A-J solver

The maximum error occurs at r=0 and is 3.04%.

5.5 VALIDATION OF FLUENT SIMULATIONS ON A 3D SQUARE BAR

The Geometric properties, material properties and mesh generation have been described in Chapter 4. The boundary conditions are the same as shown in Table 4.3 except that since potential is not being solved, no boundary conditions need to be specified.

5.5.1 Results

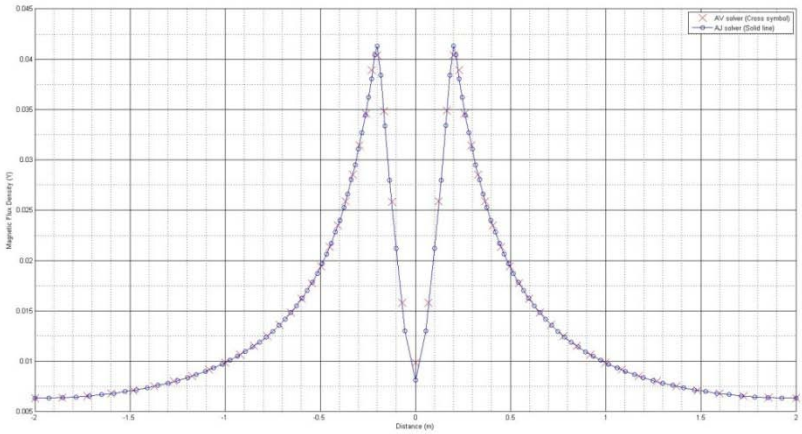

Figure 5.2: Comparison of variation of magnetic flux density along the length (x direction) computed using A-V and A-J solver

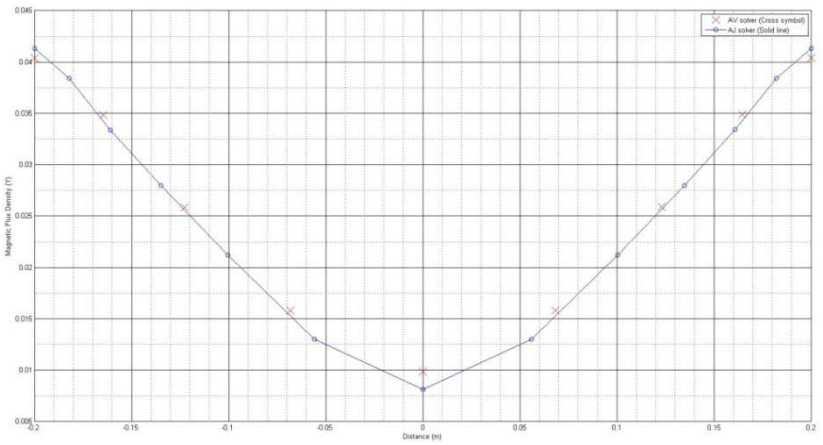

Figure 5.3: Comparison of variation of magnetic flux density inside the conductor along the length (x direction) computed using A-V and A-J solver

The error at x=0 is considerably higher (20%) which can be attributed to the error in discretization. At other points the error between the two formulations is 2%.

CHAPTER 6

SEQUENTIAL DEVELOPMENT OF ELECTROMAGNETIC STIRRER

6.1 INTRODUCTION

In Chapter 5, **AJ** formulation was described and a comparison of the results for the cases described in Chapter 4 was done. The results obtained from the **AV formulation** and **AJ** formulation was done with the results closely tallying.

In this chapter, using the previously described **AJ formulation,** the magnetic field around a circular current carrying ring is computed at any point. The thesis by Milind [13] has been used in this chapter for validating the results. This validation serves as the cornerstone for further work.

In practice, three phase currents are applied to phase displaced coils to generate a travelling magnetic field. To get further insight into the details of the generation of travelling magnetic field, current sheet concept is used where the flow of current is thought to be in sheets along the axis of the solenoid. Subsequently, the magnetic field around a solenoid carrying a constant current, space varying current, time varying current and both spatially and time varying current is found. This bottom up approach to modeling a linear electromagnetic stirrer gives insight in understanding the generation of a travelling magnetic field which gives rise to induced eddy currents and thereby Lorentz forces which we seek to compute.

6.2 VALIDATION OF FLUENT SIMULATIONS OF A CIRCULAR COIL CARRYING CURRENT

6.2.1 Geometric Properties

Table 6.1 shows the details of the computational domain.

Table 6.1: Geometric details of computational domain

Radius (m)	Height (m)	Applied Current density (A/m^2)
0.05	0.24	225 e3

Using the data given in [13], the coil is modeled as shown in Figure 6.1. The geometric details are shown in Table 6.2

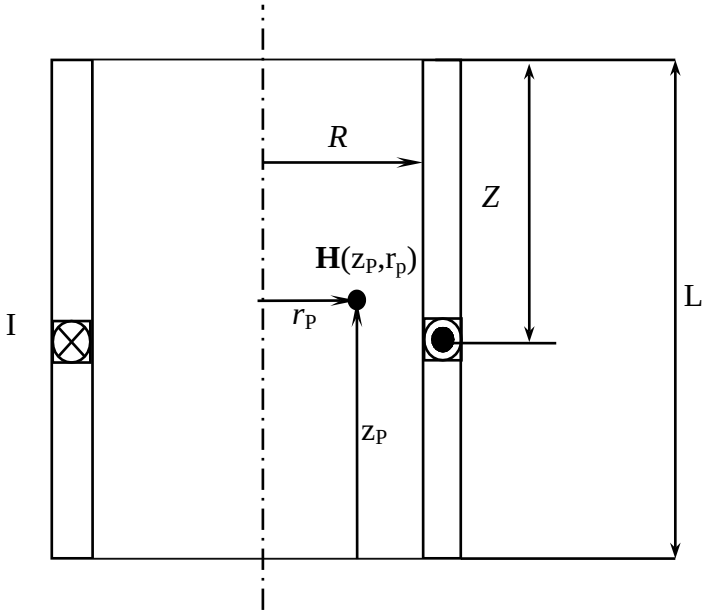

Figure 6.1: Coil configuration

The analytical solution as mentioned in [21] is given as

$$H_z(z_p, r_p, z) = \frac{NRI}{4\pi}\left(\int_0^{2\pi} \frac{(R - r_p\cos\phi)}{\left[r_p^2 + R^2 - 2Rr_p\cos\phi + (z_p - z)^2\right]^{\frac{3}{2}}} d\phi\right) \quad (6.1)$$

$$H_r(z_p, r_p, z) = \frac{NRI}{4\pi}\left(\int_0^{2\pi} \frac{(z - z_p)\cos\phi}{\left[r_p^2 + R^2 - 2Rr_p\cos\phi + (z_p - z)^2\right]^{\frac{3}{2}}} d\phi\right) \quad (6.2)$$

Here, $H_z(Z_p,0, 0)$ indicates the axial field at various Z_p for $R_p = 0$ when the current carrying coil is located at Z=0.0.

Table 6.2: Geometric details of coil

Inner radius (m)	Outer Radius (m)	Mean Radii (m)	Thickness (m)	Magnetic Permeability (Wb/m)
0.038	0.042	0.04	0.01	1.26 e-6

6.2.2 Mesh

Meshing of the cylindrical computational domain is done using ICEM 14.0 [22]. A hexahedral mesh was used as shown in Figure 6.2.

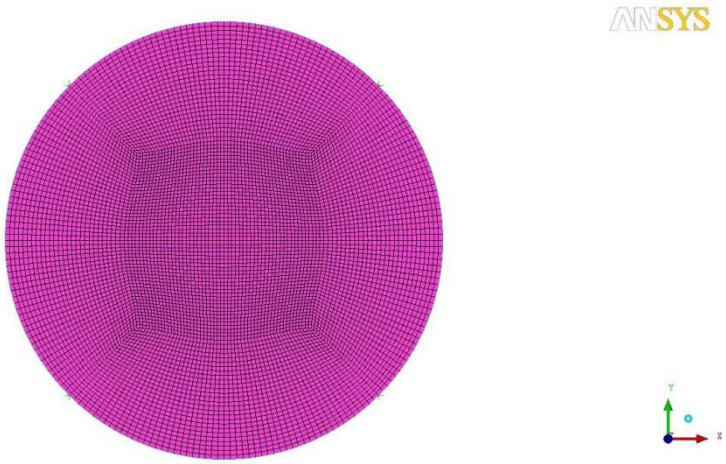

Figure 6.2: Meshing of cylindrical domain in ICEM CFD

6.2.3 Results

The variation of magnetic field strength along the axis shown in Figure 6.3.

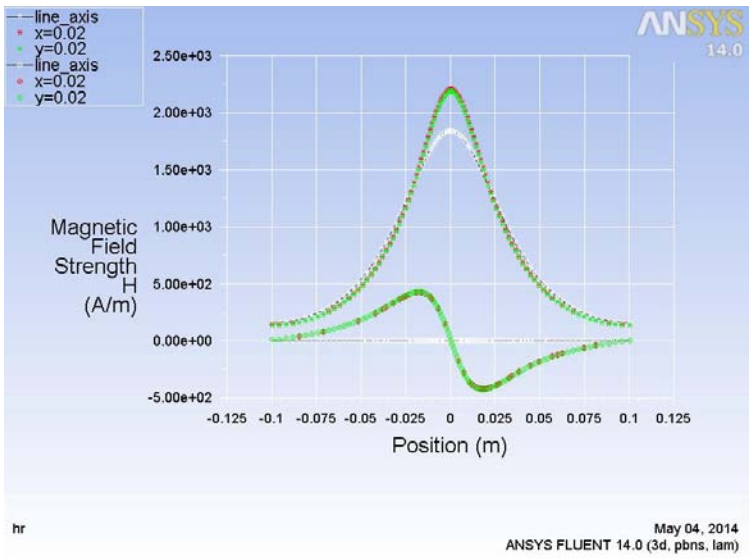

Figure 6.3: Variation of magnetic field strength along the axis

It can be seen that the magnitude of Axial magnetic field is higher than the magnitude of radial magnetic field. Along the axis of the cylindrical domain there is no radial magnetic field from symmetry considerations. For a line drawn in the XZ plane along the axis, Y component of magnetic field is zero and for a line drawn in

the YZ plane along the axis, the plane the X component of magnetic field is zero. This follows from applying Biot- Savart Law [23].

The contours of current density and magnetic field vectors on the slice plane along the axis through the center of the domain viewed from the top (X direction) are shown in Figure 6.4. The formation of closed loops of magnetic field lines can be observed near the coil.

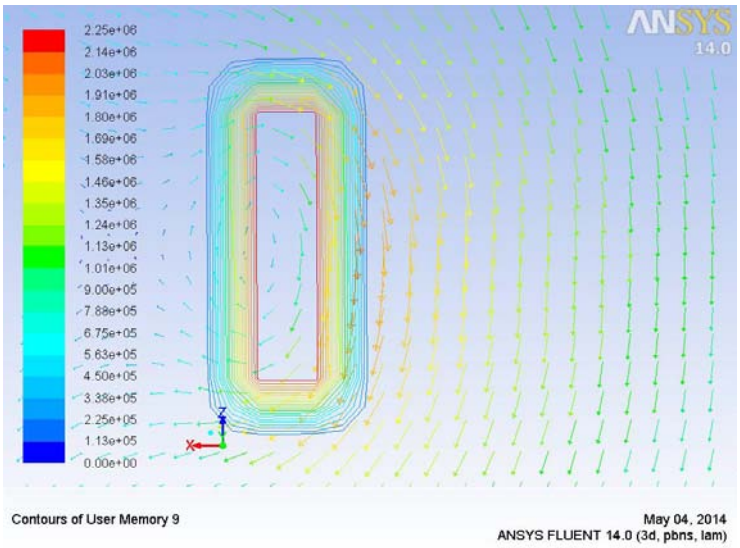

Figure 6.4: Contours of current density and magnetic field vectors on the slice plane along the axis through the center of the domain viewed from the top (X direction)

6.3VALIDATION OF FLUENT SIMULATIONS OF A SOLENOID CARRYING CONSTANT CURRENT

6.3 1 Geometric details

The solenoid configuration is given in Figure 6.5. The geometric details of the solenoid are shown in Table 6.2. The solenoid is modeled as a set of rings closely spaced.

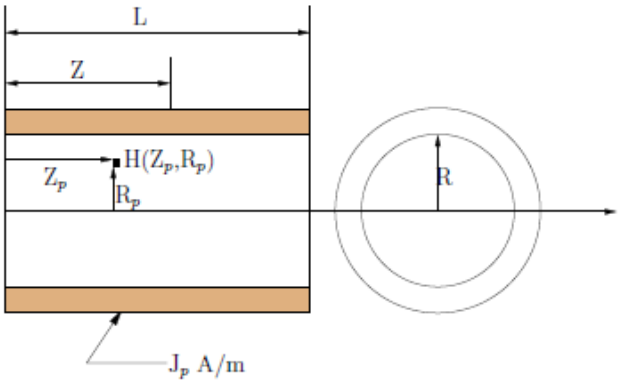

Figure 6.5: Solenoid configuration

The analytical solution given in [21] is

$$H_z\left(z_p,r_p,t\right)=\frac{RJ}{4\pi}\int_0^L\int_0^{2\pi}\left(\frac{\left(R-r_p\cos\varphi\right)}{\left[r_p^2+R^2-2Rr_p\cos\varphi+\left(z_p-z\right)^2\right]^{\frac{3}{2}}}d\varphi\right)dz \qquad (6.3)$$

$$H_r\left(z_p,r_p,t\right)=\frac{RJ}{4\pi}\int_0^L\int_0^{2\pi}\left(\frac{\left(z-z_p\right)\cos\varphi}{\left[r_p^2+R^2-2Rr_p\cos\varphi+\left(z_p-z\right)^2\right]^{\frac{3}{2}}}d\varphi\right)dz \qquad (6.4)$$

Table 6.3: Geometric details of solenoid

Inner radius (m)	Outer Radius (m)	Mean Radii (m)	Thickness (m)
0.038	0.042	0.04	0.2

6.3.2 Mesh

The details of the mesh are the same as those for the coil.

6.3.3 Results

The variation of magnetic field strength along the axis is shown in Figure 6.6. It can be seen that the axial magnetic field is nearly constant along the height of the solenoid and the radial magnetic field is negligible. Thus, the field is predominantly axial. The radial field is negligible along the axis of the solenoid but is prominent at its ends. This is known as the end effect.

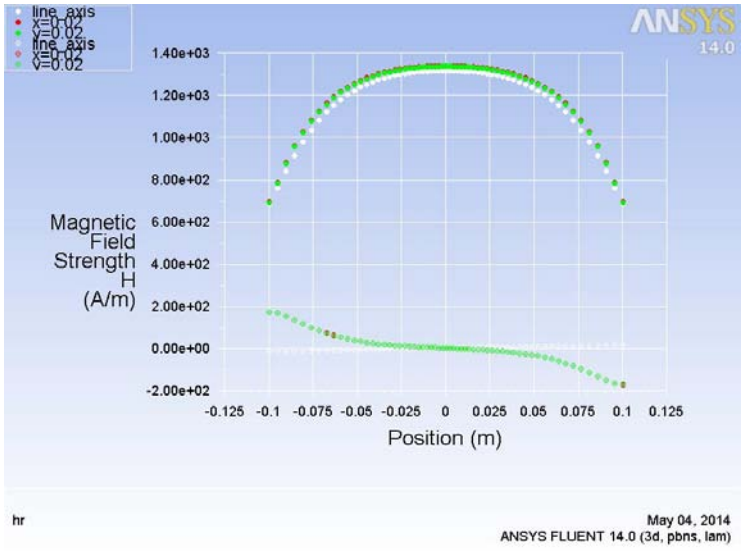

Figure 6.6: Variation of magnetic field strength for a solenoid along the axis

The contours of current density and magnetic field vectors on the slice plane along the axis through the center of the domain viewed from the top (X direction) are shown in Figure 6.7. The contour of the current density resembles a sheet of current and the magnetic field lines are nearly parallel to the axis inside the solenoid.

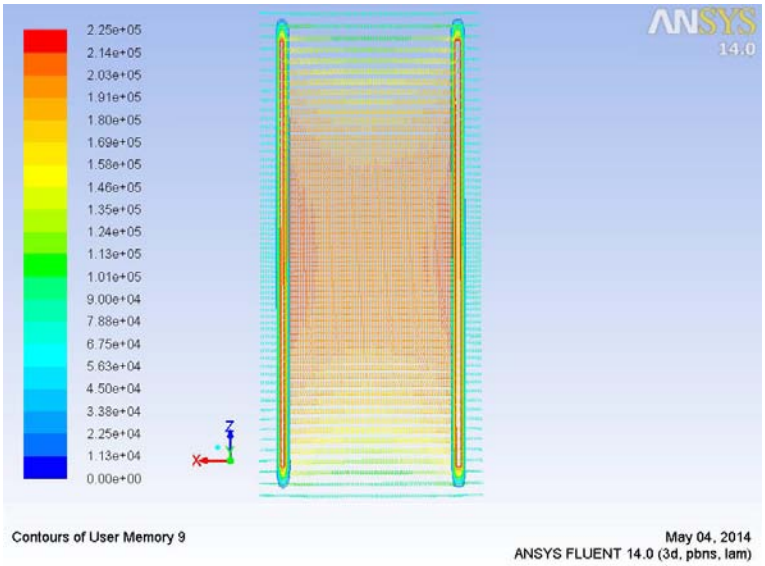

Figure 6.7: Contours of current density and magnetic field vectors on the slice plane along the axis through the center of the domain viewed from the top (X direction)

6.4VALIDATION OF FLUENT SIMULATIONS OF A SOLENOID SPATIALLY VARYING CURRENT

The space varying current is given as $J_p = J \sin\left(\frac{2\pi z}{L}\right)$ (6.5)

Where Z is in the axial direction

6.4.1 Geometric details

The solenoid configuration is given in Figure 6.5.The geometric details are shown in Table 6.2.
The analytical solution given in [21] is:

$$H_z\left(z_p, r_p, t\right) = \frac{RJ}{4\pi}\int_0^L\int_0^{2\pi}\left(\frac{\left(R - r_p\cos\varphi\right)\sin\left(\frac{2\pi z}{L}\right)}{\left[r_p^2 + R^2 - 2Rr_p\cos\varphi + \left(z_p - z\right)^2\right]^{\frac{3}{2}}}d\varphi\right)dz \quad (6.6)$$

$$H_r\left(z_p, r_p, t\right) = \frac{RJ}{4\pi}\int_0^L\int_0^{2\pi}\left(\frac{\left(z - z_p\right)\cos\varphi\sin\left(\frac{2\pi z}{L}\right)}{\left[r_p^2 + R^2 - 2Rr_p\cos\varphi + \left(z_p - z\right)^2\right]^{\frac{3}{2}}}d\varphi\right)dz \quad (6.7)$$

6.4.2 Mesh

The mesh details are the same as those for the coil.

6.4.3 Results

The vectors of current density in the solenoid are shown in Figure 6.8. It can be seen from equation (6.5) that the wavelength is equal to the height of the solenoid.

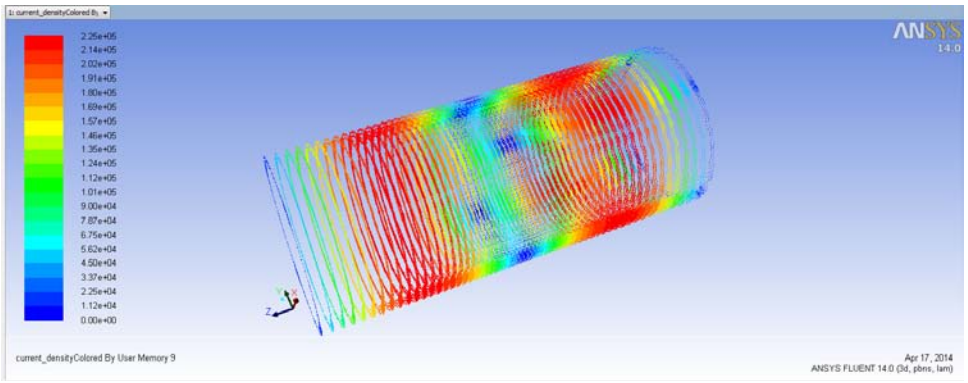

Figure 6.8: Primary Current density vectors in the solenoid

For a solenoid the L/R ratio (length of the solenoid to its mean radius) determines the magnitude of the radial and axial magnetic field. This magnitude of axial and radial magnetic field strength for different L/R ratio is studied and shown in Figure 6.9, Figure 6.10 and Figure 6.11. With increasing L/R ratio, the magnitude of axial magnetic field

strength increases whereas the magnitude of radial magnetic field strength decreases. It can be seen that the magnetic field is travelling in space i.e., along the length of the solenoid.

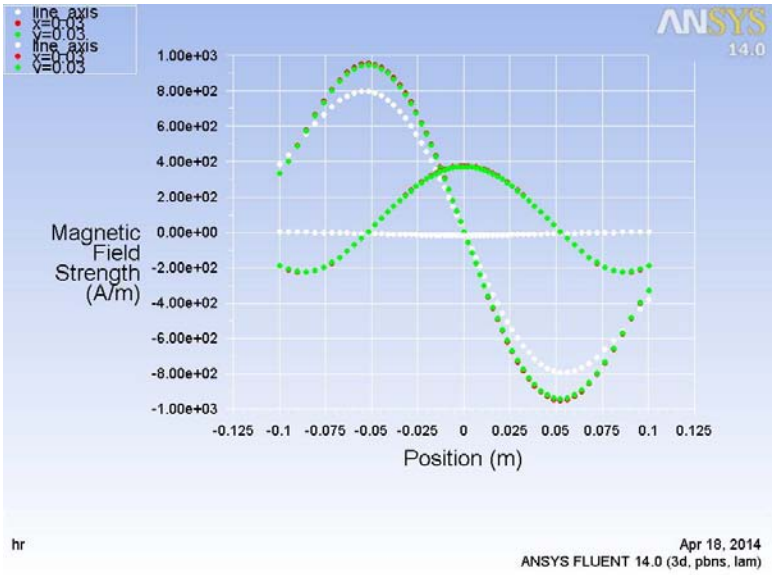

Figure 6.9: Variation of Magnetic field strength along the axis for L/R =5

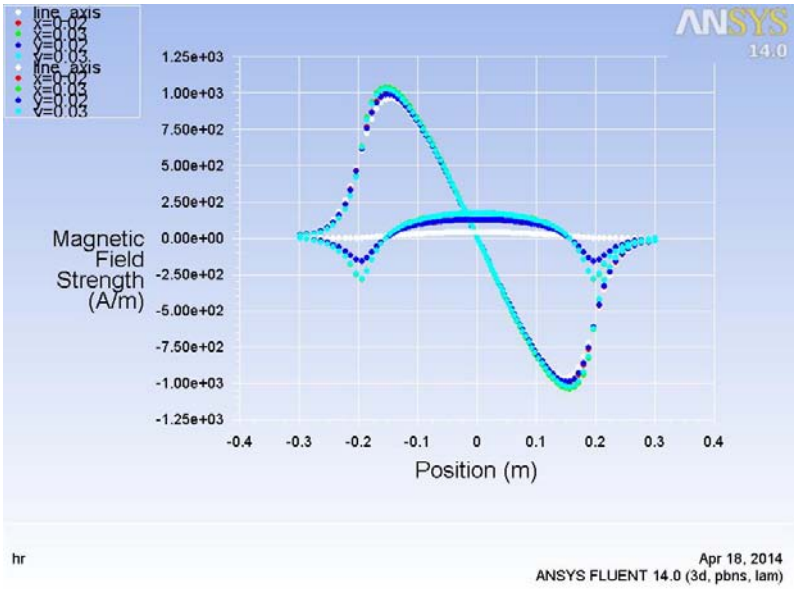

Figure 6.10: Variation of Magnetic field strength along the axis for L/R =10

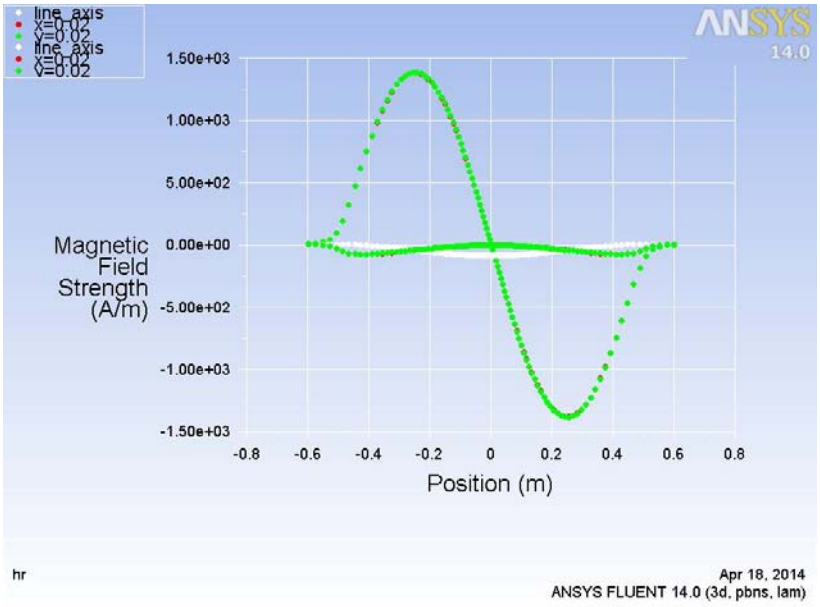

Figure 6.11: Variation of Magnetic field strength along the axis for L/R =25

6.5 VALIDATION OF FLUENT SIMULATIONS OF A SOLENOID CARRYING TIME VARYING CURRENT

Consider a case where a conducting liquid or a bar is placed inside the solenoid. For the generation of induced or eddy currents, there has to be a time rate of change of magnetic flux linked with the conducting liquid or bar. Thus, in essence a time varying field is essential to give rise to induced currents and thus generate Lorentz force.

The time varying current is given as $J_p = J \sin(\omega t)$ (6.8)

The frequency of alternating current density is 50 Hz. The time period is 0.02 s.

6.5.1 Geometric details

The solenoid configuration is given in Figure 6.5.The geometric details are shown in Table 6.2. To compute the induced current density and a Lorentz force, a conductor of high magnetic relative magnetic permeability is kept inside the solenoid. The dimensions of the conductor and its material properties are given in Table 6.3.

Table 6.3: Geometric details of cylindrical bar inside the solenoid

Inner radius (m)	Outer Radius (m)	Centre	Thickness (m)	Relative Magnetic Permeability of bar (Wb/m)
0.0	0.02	(0.0,0.0,0.0)	0.1	2000

The analytical solution given in [21] is:

$$H_z\left(z_P, r_P, t\right) = \frac{RJ}{4\pi}\int_0^L \int_0^{2\pi} \left(\frac{\left(R - r_P \cos\varphi\right)\ \sin\left(\omega t\right)}{\left[r_P^2 + R^2 - 2Rr_P\cos\varphi + \left(z_P - z\right)^2\right]^{\frac{3}{2}}} d\varphi \right) dz \qquad (6.9)$$

$$H_r\left(z_P, r_P, t\right) = \frac{RJ}{4\pi}\int_0^L \int_0^{2\pi} \left(\frac{\left(z - z_P\right)\ \cos\varphi \sin\left(\sin\ \omega t\right)}{\left[r_P^2 + R^2 - 2Rr_P\cos\varphi + \left(z_P - z\right)^2\right]^{\frac{3}{2}}} d\varphi \right) dz \qquad (6.10)$$

6.5.2Mesh

The mesh details are the same as those for the coil.

6.5.3 Results

Grid independence test is carried out for different cell sizes. The parameters which are most affected by cell size are:

1. Axial Magnetic field along the radius and height
2. Magnitude of Lorentz force and Induced current density along the radius

The time taken is t=0.005 s because at this value the primary current density reaches its maximum value. These parameters are used to test grid independence.

Figure 6.12 shows the radial and axial variation of Magnetic field strength with the number of cells.

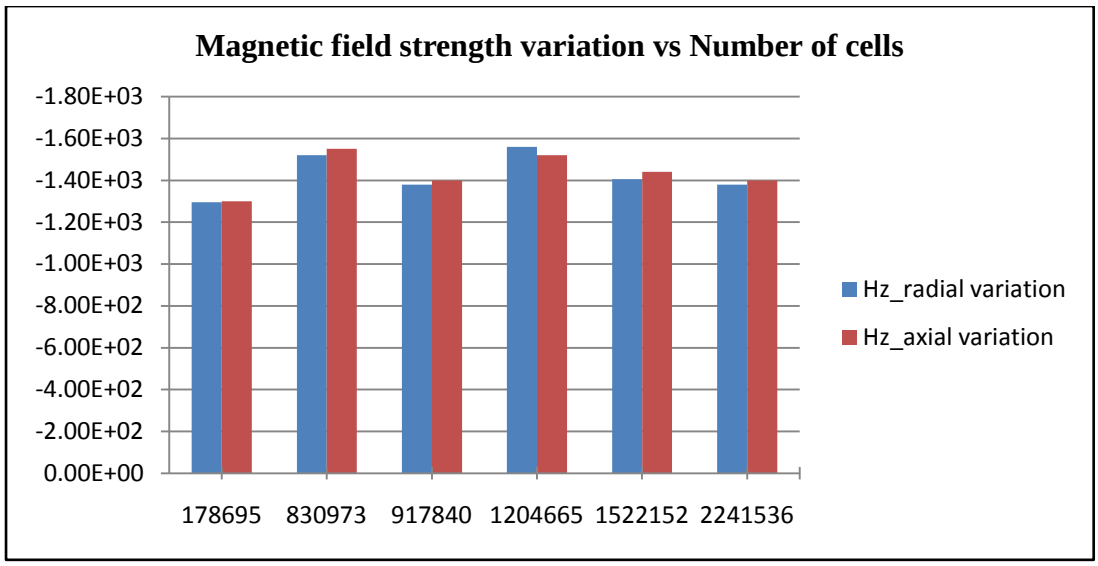

Figure 6.12: Radial and axial variation of Hz (A/m) with number of cells

Figure 6.13 and Figure 6.14 show the radial variation of induced eddy current and Lorentz force with number of cells.

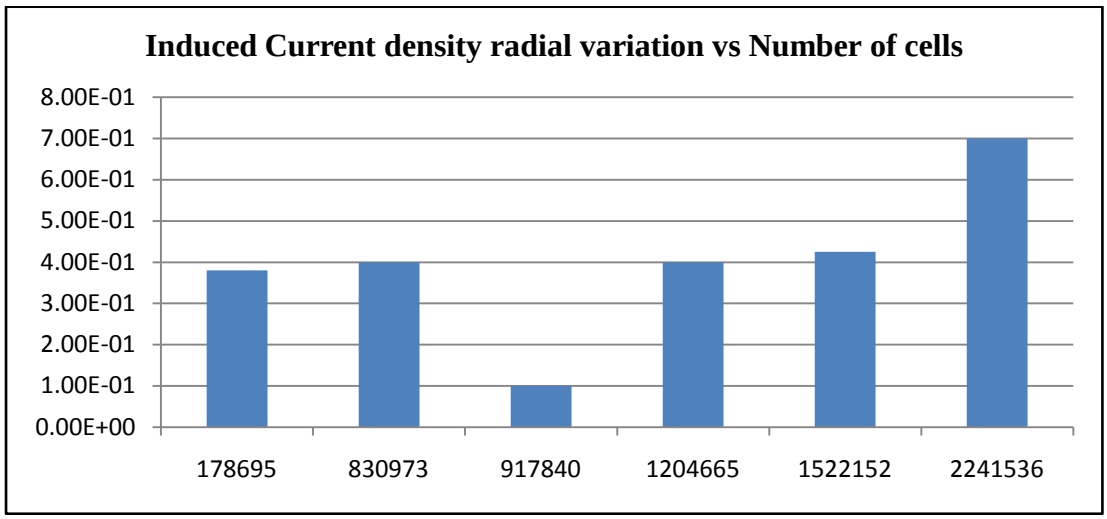

Figure 6.13: Radial variation of induced current density with number of cells

Considering the computational limitations and the near constant variation of axial component of magnetic field, the number of cells is taken as 2241536.

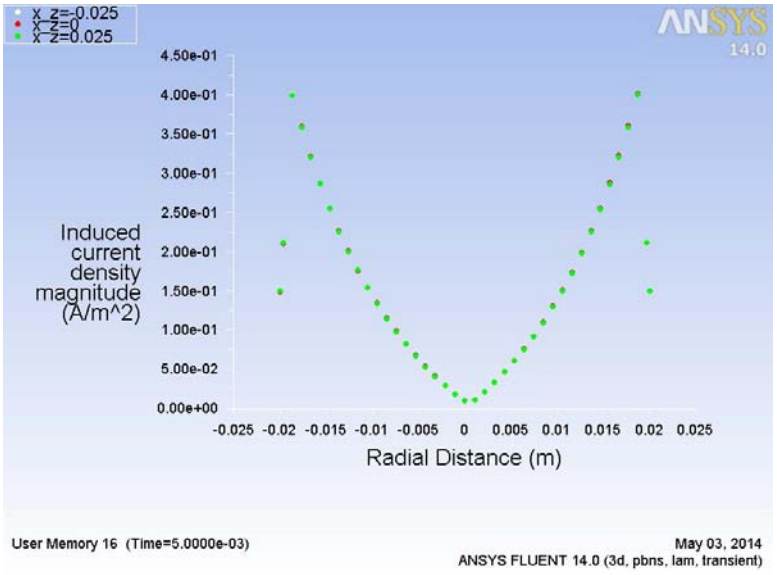

Figure 6.14: Variation of Lorentz force magnitude along the radial direction

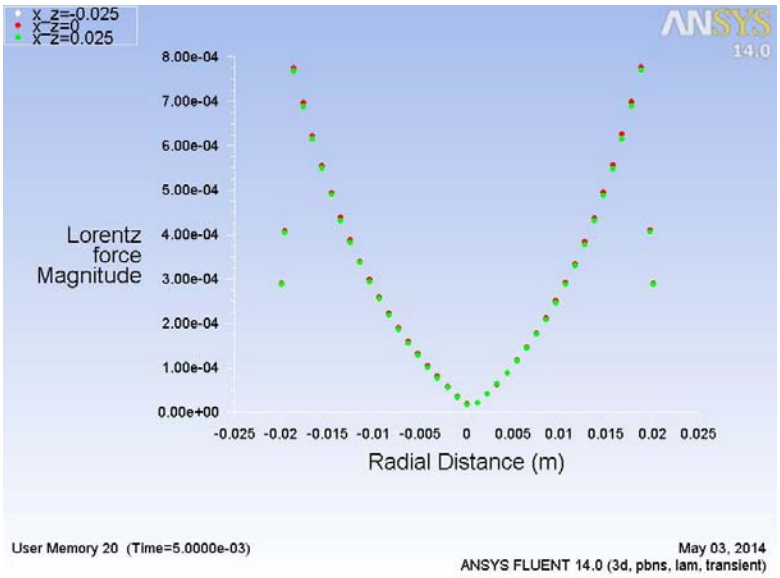

Figure 6.15: Variation of Lorentz force magnitude along the radial direction

From Figure 6.14 and Figure 6.15, it can be seen that the magnitude of the Induced current density and Lorentz force is maximum on the surface of the conductor. The eddy currents that are formed are concentric with the cylinder. Figure 6.16 shows the radial variation of radial component of Lorentz force. It is seen by comparing by Figure 6.15 and Figure 6.16 that the magnitude of radial force is almost equal to magnitude of Lorentz force. Thus, magnitude of axial component of Lorentz force is less.

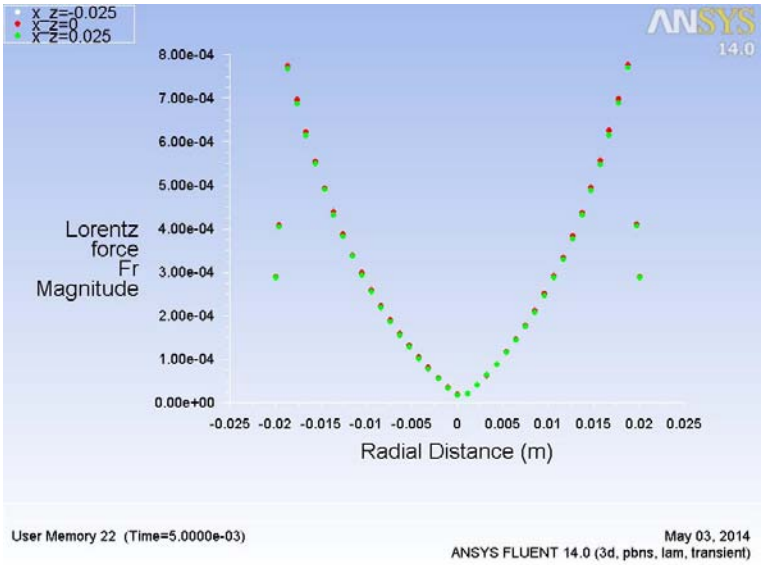

Figure 6.16: Variation of radial component of Lorentz force along the radial direction

Figure 6.17 shows the contours of induced current density and applied primary current superimposed on Lorentz force vectors at t=0.005s (when the magnitude of applied current density is maximum) and at t=0.02 s.

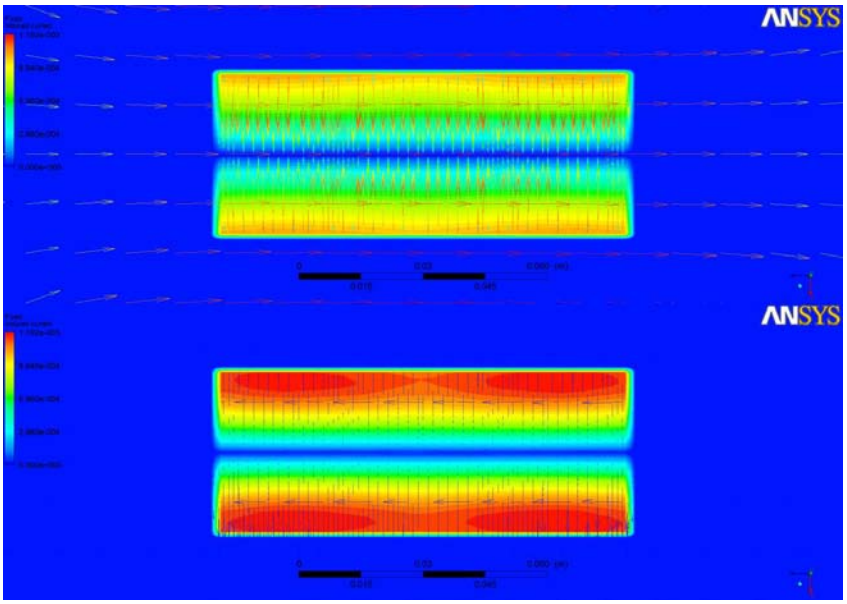

Figure 6.17: Contours of induced current density and applied primary current superimposed on Lorentz force vectors at t=0.005s and t=0.02 s

In Figure 6.17, the horizontal axis is the Z axis. The direction of current at t=0 s is clockwise when viewed from the left. Thus, the direction of magnetic field at t=0 is towards negative Z. The direction of magnetic field gets reversed after t=0.01 s.

This gives further insight into understanding the mechanism of stirring action. The radial component of Lorentz force is responsible for gripping the fluid and the axial component of the Lorentz force transports the fluid along the axis.

This is similar to Peristalsis – symmetrical contraction and expansion of muscles that occur in digestive tract. However, in this case the radial field is just time varying and not space varying. Thus, the Lorentz force vectors oscillate about the mean position with time. Thus, a combination of space and time varying field needs to be generated. Figure 6.18 shows the variation of magnetic field strength along the axis.

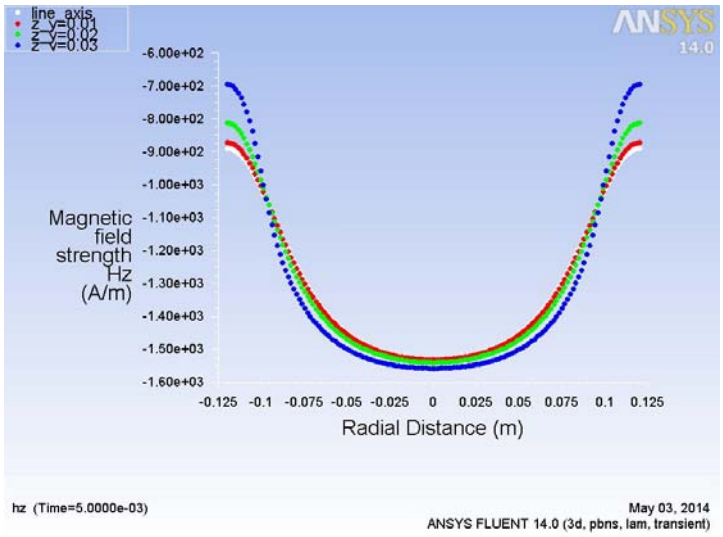

Figure 6.18: Variation of Magnetic field strength H_z along the axis

6.6. VALIDATION OF FLUENT SIMULATIONS OF A SOLENOID CARRYING TIME AND SPATIALLY VARYING CURRENT

In practice, to create a travelling magnetic field in the stirrer, a current varying in time and space needs to be applied. This is a combination of article 6.3 and article 6.4. In article 6.3, a spatially varying current gave rise to a spatially varying magnetic field inside the solenoid. However, this field is not enough to generate Lorentz force in a conductor placed inside the solenoid. In article 6.4, a time varying field was applied which gave rise to a time varying magnetic field inside the solenoid resulting in the generation of Lorentz forces. A combination of these two cases results in the generation of time and spatially varying fields which is equivalent to a three phase supply.

The spatially and time varying current density is given as

$$J_z = J_p \sin\left[\frac{2\pi z}{L} - \omega t\right] \qquad (6.11)$$

6.6.1 Geometric properties

The solenoid configuration is given in Figure 6.5.The geometric details are shown in Table 6.2. To compute the induced current density and a Lorentz force, a conductor of high magnetic relative magnetic permeability is kept inside the solenoid. The dimensions of the conductor and its material properties are given in Table 6.3.

6.6.2 Mesh

The mesh details are the same as those for the coil.

6.6.3 Results

Figure 6.19 and Figure 6.20 shows the variation of the Lorentz force at t=0.005s and at t=0.002 s (end of cycle). It can be seen that a travelling field (in space) is generated as the peak of the Lorentz force changes with time. However, there is a sign reversal in the force field vectors which is not desirable for stirring as the mechanism of stirring is similar to peristaltic effect – hence the conducting liquid needs to be gripped and then transported along the axis. This is achieved by use of three phase currents.

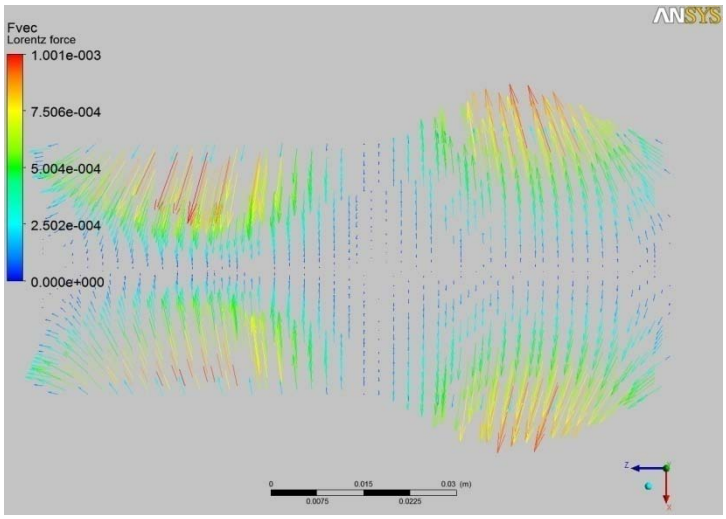

Figure 6.19: Lorentz force vectors at t=0.005s

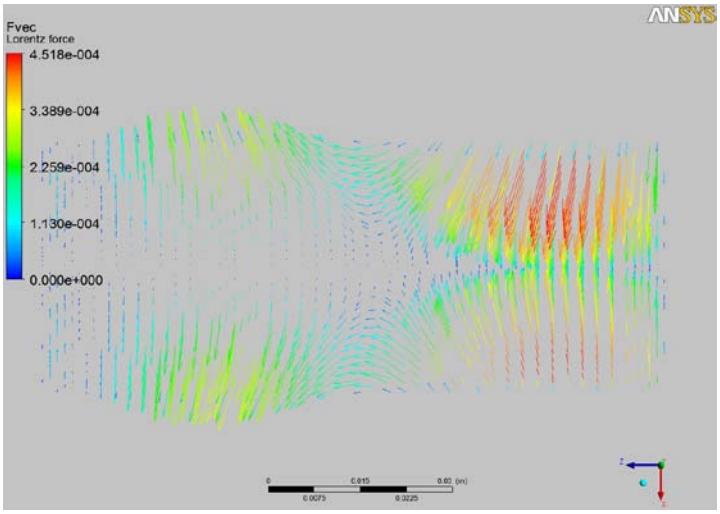

Figure 6.20: Lorentz force vectors at t=0.005s

Figure 6.21 shows the travelling magnetic field.

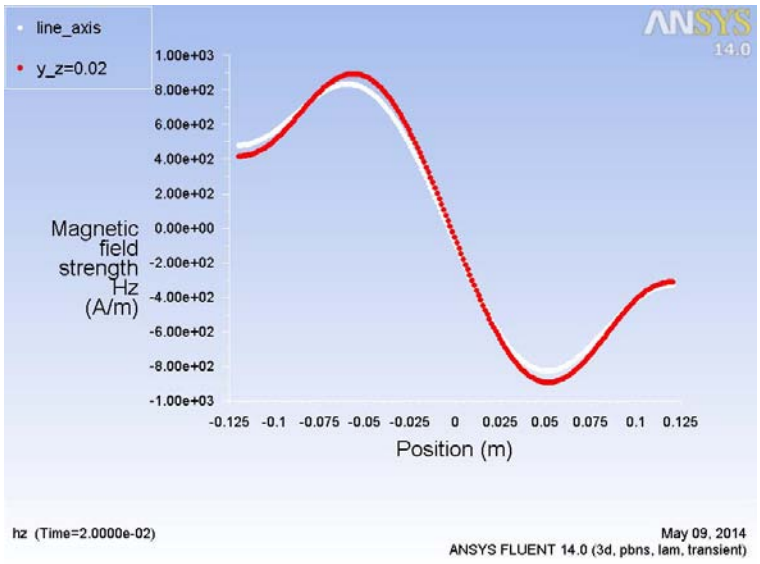

Figure 6.21: Variation of Magnetic field strength H_z along the axis

CHAPTER 7

DESIGN OF LINEAR ELECTROMAGNETIC STIRRER

7.1 INTRODUCTION

Figure 7.1 (a) shows the structure of a linear electromagnetic stirrer. The coils AA$^{|}$, BB$^{|}$, CC$^{|}$ are arranged in a linear fashion to form the stator windings. These coils are displaced in space by $L/6$ (m) where L is the total length of the stirrer. The coils A$^{|}$, B$^{|}$, C$^{|}$ carries same currents as coils A, B and C, respectively, but in opposite directions. The phasor representation of the currents at a particular instance is shown in Figure 7.1 (b). The above coil arrangement, when excited by a three phase alternating current, generates sinusoidally distributed magneto motive force (mmf) in space as well as time. The resulting mmf establishes a magnetic field $\mathbf{H}(r,z,t)$ travelling along the axis of the stirrer. The variation of the axial field induces voltage $\mathbf{E}(\phi)$ in the molten metal in the tangential direction. As a result of the induced voltage, a tangential eddy current field $\mathbf{J}(\phi)$, is created. The interaction of the tangential eddy currents $\mathbf{J}(\phi)$ and induced magnetic field, $\mathbf{B}(r,z)$, in the metal generate axial and radial forces $F_z(r, z, t)$ and $F_r(r, z, t)$, respectively, in the metal. The molten metal convects under the influence of these forces.

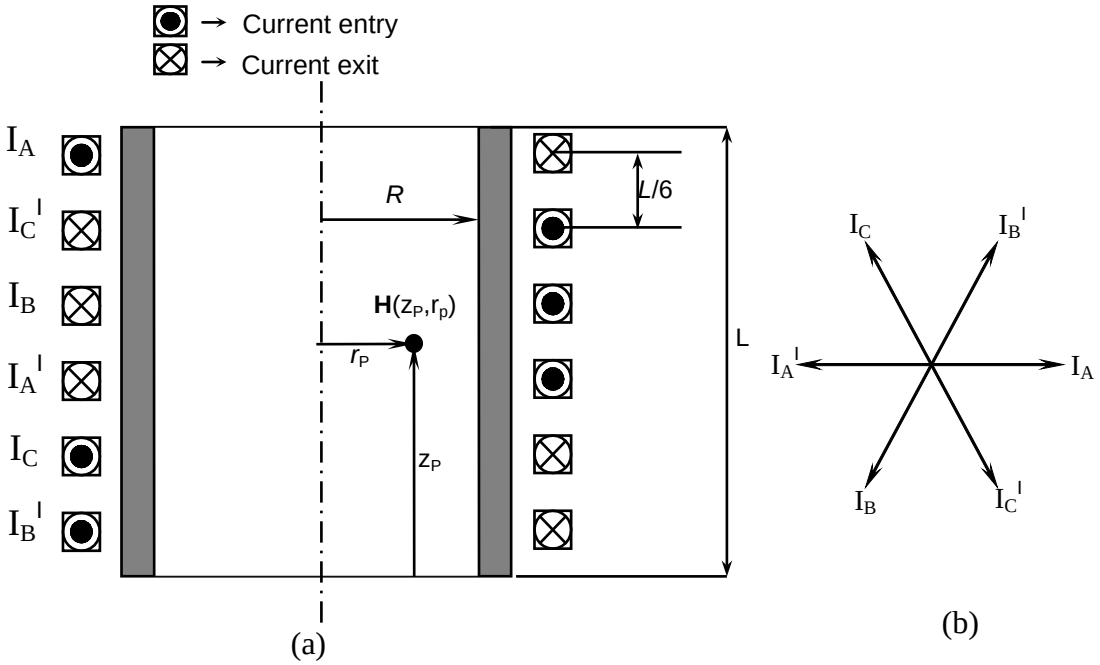

Figure 7.1 (a) Coil arrangement in a two pole in a LEMS

Figure 7.1 (b) Phasor notation of currents.

7.2 MAGNETIC FIELD CALCULATIONS

As evident from the previous discussion, the magnetic field set up by the primary current is the first step in the calculation of Lorentz force.

Let f be the frequency of the sinusoidally distributed three-phase primary excitation current in the stator. Since L>>R (L- length of the stirrer and R- inner radius of the coil), the three-phase stator current can be approximated to a current sheet having a linear current density $J_p \sin\left(\omega t - \frac{2\pi z}{L}\right)$ travelling at an average velocity of Lf m/s. The current sheet is developed by obtaining the lumped currents in each individual phase coils, as schematically represented in Figure 7.2.

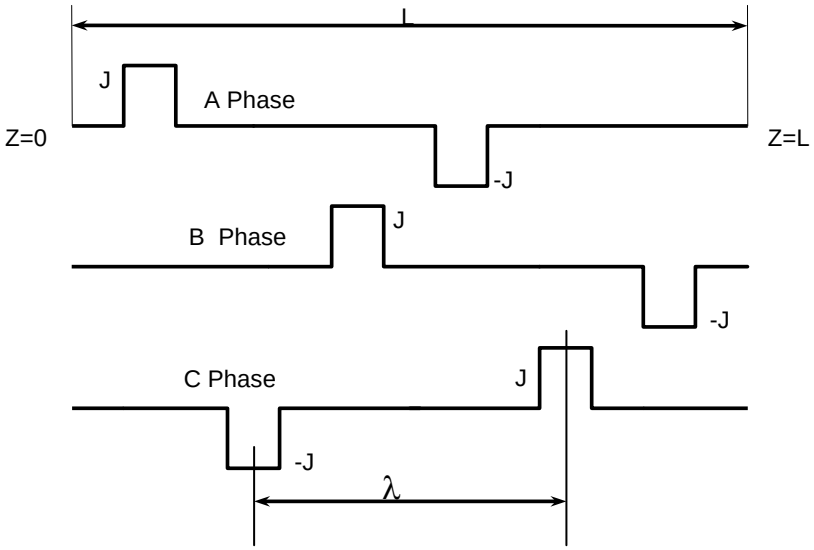

Figure 7.2: Three phase lumped currents in the coils

Details on the development of current sheet from preliminaries for a linear stirrer are explained in [24].

7.3 MODELING OF LINEAR ELECTROMAGNETIC STIRRER USING THREE PHASE CURRENTS

Adopting a bottom up approach for modeling linear electromagnetic stirrer, the height of the stirrer (along the axis) is divided into three equal parts with each segment carrying one phase. The results obtained are discussed below. Figure 7.3 shows the current density vectors viewed from positive X axis at t=0.005. Three distinct phase shifted rings of current can be seen.

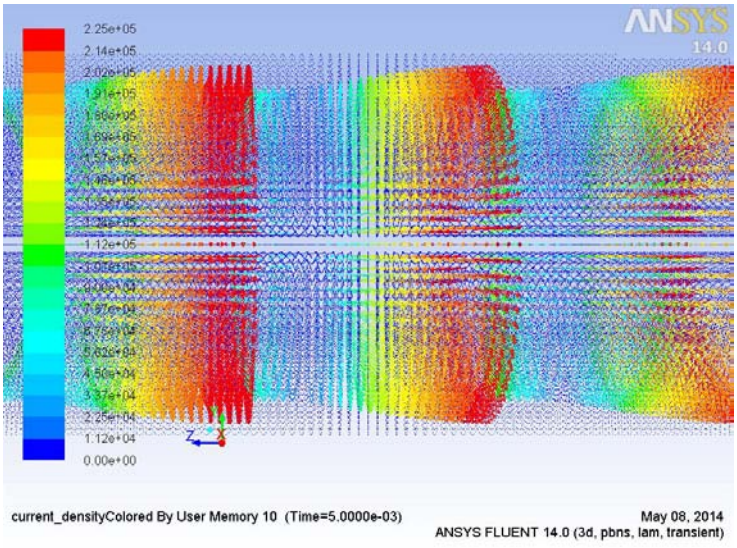

Figure 7.3: Applied current density vectors

Vectors of Lorentz force are shown in Figure 7.4. It can be seen that they are primarily in the radial direction. Joining the heads of these vectors, a sinusoidal wave can be seen. Design of a linear electromagnetic stirrer involves controlling the direction and magnitude of these generated forces. The Lorentz forces are responsible for the convection of the conducting liquid or cylindrical bar.

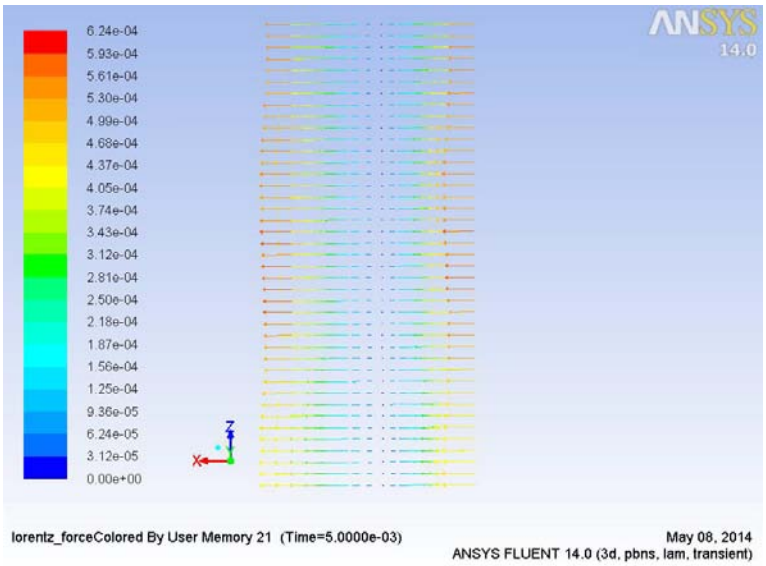

Figure 7.4: Lorentz force vectors

CHAPTER 8

CONCLUSION

In this thesis, an attempt has been made to tackle the problem of designing a Linear Electromagnetic stirrer. The initial part of this thesis focuses on exploiting the huge calculation potential of FLUENT commercial solver to solve static electromagnetic field problems. A close fit is obtained between the analytical and computational results. In the long run, these validation cases can be applied to analyze and design complex electromagnetic devices such as electrical machines or to areas like electromagnetic pumping.

A bottom up approach to design the linear electromagnetic stirrer is adopted. The stirrer is modeled using the Current sheet concept which gives an insight into the mechanism of stirring. To improve the accuracy of the model, an attempt has been made to incorporate three phase currents instead of the current sheet concept.

Due to the time limitations of the thesis work, several interesting areas are left to be explored. The effect of magnetic return paths which are tooth shaped structures of high magnetic permeability which are inserted between coils to prevent leakage of flux lines outside the stirrer and the coupling of electromagnetic equations and the momentum equations are two important study directions. Subsequently, the solidification/melting module can be implemented to track the solidification and melt front as the primary application of electromagnetic stirrer is in rheocasting or continuous casting. It is hoped that this thesis serves as a foundation work for designing linear electromagnetic stirrer.

REFERENCES

1. **C., Flemings M.** *Solidification Processing*. : McGraw-Hill, 1974.

2. *Behavior of metal alloys in the semisolid state.* **Flemings M. C.** 1991, Metallurgical Transactions, pp. 269-293,.

3. *The effect of electromagnetic stirring during solidification on the structure of Al-Si alloys.* **Griffiths, W. D. and McCartney, D. G.** 1996, Materials Science and Engineering, Vol. 216(1), pp. 47-60.

4. *Effects of electromagnetic stirring during the controlled solidification of tin.* **Vives, C. and Perry, C.** 1986, International journal of heat and mass transfer, Vol. 29(1), pp. 21-33.

5. **Davidson, P. A.** *An introduction to magnetohydrodynamics*. : Cambridge university press, 2001. Vol. 25.

6. **Moffatt, H K.** *Magnetic field generation in electrically conducting fluids* : Cambridge University Press, 1978.

7. **Moreau, R.** *Magnetohydrodynamics*. : Kluwer Acad. Pub, 1990.

8. **Shercliff, J A.** *A textbook of magnetohydrodynamics.* : Pergamon Press, 1965.

9. *Electromagnetic stirring in continuous casting of steel.* **Marr, H. S.** 1982, Metallurgical Applications of Magnetohydrodynamics, pp. 143-153.

10. *Electromagnetic stirring and continuous casting—Achievements, problems, and goals.* **Tzavaras, A. A. and Brody, H. D.** 1984, Journal of Metals, Vol. 36(3), pp. 31-37.

11. *On the calculation of the electromagnetic force field in the circular stirring of metallic melts.* **Saluja, N., Ilegbusi, O. J. and Szekely, J.** 1990, Journal of applied physics,, Vol. 68(11), pp. 5845-5850.

12. *Experimental and computational investigation of rotary electromagnetic stirring in a woods metal system.* **Partinen, et al.** 1994, ISIJ international, Vol. 34, pp. 707-707.

13. *Design and analysis of a linear type electromagnetic stirrer. In Industry Applications.* **Milind, S., and Ramanarayanan.** s.l. : IEEE, 2004, Vol. 1.

14. *Studies on transport phenomena during solidification of an aluminum alloy in the presence of linear electromagnetic stirring.* **Barman, N., Kumar, P., and Dutta, P.** 2009, Journal of Materials Processing Technology, Vol. 209(18), pp. 5912-5923.

15. *Fluent 12.1 User Manual.* : ANSYS INC.

16. *12.0: UDF MANUAL*. : ANSYS FLUENT, 2009.

17. *Plasma arc welding simulation with OpenFOAM.* **Sass-Tisovskaya, Margarita.** 2009.

18. *OpenFOAM Simulation for Electromagnetic Problems.* **Huang, Zhe.** 2010.

19. *Modelling of dynamic arc behaviour in a plasma reactor.* **Westermoen, Andreas.** : NTNU, 2007.

20. *Mathematics Applied to Electrical engineering.* **Warren, Aurthur George.**. : Chapman and Hall, 1942.

21. *Numerical Methods in Electromagnetism.* **Chari, M. V. K. and Salon, S. J.**. : Academic Press, 2000.

22. *ICEM CFD 11.0 User Manual*.. : ICEM, 2007.

23. *Introduction to electrodynamics.* **Griffiths, D. J.** : Prentice Hall, 1999, Vol. 3.

24. *Development of a Linear Electromagnetic Stirrer for Rheocasting of Aluminium alloys* . **Kumar, Pramod.**. : Indian Institute of Science, 2008.

Biography

Yash Ganatra was born on 11 August, 1992 in Bombay (now Mumbai). His ambitions for the future included being a professional football player, being a rocket scientist. What fascinated him was the work his father did – designing fluidized bed boilers. His interest in thermal fluid sciences stems from this fact.

He belonged to the first batch in school, entered high school during its 25th year and at present he belongs to the first batch of Vellore Institute of Technology-Chennai and was part of the first team from the campus that developed a car. He hopes to attend graduate school one day and believes that there are many more first to come

His interests include outside academics include supporting Arsenal Football club and reading books and doing things that make a difference.

For his current contact address, see his webpage - https://sites.google.com/site/yyashganatra/home